DEPARTMENT OF THE INTERIOR

U.S. GEOLOGICAL SURVEY

An Atlas of Facies Microfabrics of the Bootlegger Cove Formation Using the Scanning Electron Microscope

by

Randall G. Updike[1] and Robert L. Oscarson[2]

Revised 10 November 1986

Open-File Report 87-60

[1] Alaska Division of Geological and Geophysical Surveys, Eagle River, Alaska

[2] U.S. Geological Survey, Menlo Park, California

General Statement

Among the numerous phenomena initiated by the 1964 Prince William Sound Earthquake, the several catastrophic landslides in the Anchorage area (fig. 1) are among the most commonly cited. In the 20 years subsequent to that earthquake, these landslides still prevail as a major concern to geologists, engineers, and the general public. Serious ramifications result if similar slides are to occur in the future in a city which is now far more urbanized than in 1964.

It is clear from several early geotechnical studies (e.g., Shannon and Wilson, 1964; Hansen, 1965; Seed and Wilson, 1967; Kerr and Drew, 1965) that the cause of all of the major Anchorage landslides was subsurface soil failures within the Bootlegger Cove Formation. Opinion, however, has differed on the mechanism of failure. Cyclic liquefaction of sands and strength degradation of sensitive clays have been proposed in the literature.

In the past two decades the understanding of and evaluation for liquefaction potential of noncohesive soils have advanced significantly (e.g., Seed, 1976; 1979; Youd and Perkins, 1978; Bennett and others, 1981, Seed and others, 1983). The various investigators generally agree that if a saturated, cohesionless soil (ideally a well-sorted sand or silty sand) is subjected to seismically-induced cyclic shear stresses, the soil has a tendency to densify. As a result, overburden stress is transferred to the pore water and removed from the soil particles. Because shear strength varies with the overburden stress carried by the soil particles (effective stress), the shear strength is reduced. If cyclic stresses are sustained, a peak cyclic pore-pressure ratio of 100 percent can be attained. If cyclic

stress is continued (and depending upon the density of the sand, confining pressure, and magnitude of stress cycles) the soil may be mobilized to unlimited deformation or may sustain limited strain before dilating to a stable condition. Typically, the liquefaction of a subsurface sand layer will be expressed at the surface as lateral spreading of the ground with resultant fissuring. It was this process that Seed and Wilson (1967) and Seed (1968) proposed for the large 1964 Anchorage landslides. Recent studies on the sand layers within the Bootlegger Cove Formation (Updike, 1983a, 1984; Idriss, 1985) indicate that liquefaction as the primary cause of the 1964 landslides was unlikely.

Previous reports (e.g., Shannon and Wilson, 1964; Mitchell and others, 1973) have suggested that moderate to highly sensitive clays occur within the Bootlegger Cove Formation. Sensitivity is a measure of the loss of shear strength of a clay when remolded at constant water content, expressed as a ratio of in situ shear strength to remolded shear strength. Mitchell (1976) points out that virtually all normally consolidated clays and slightly overconsolidated clays exhibit some amount of sensitivity. The most sensitive clays (quick clays) turn to a viscous fluid when remolded. Of the approximately 2100 Bootlegger Cove Formation cohesive soil samples tested immediately after the earthquake, only about 14 percent gave high to extremely high sensitivity ratios (from 10 to greater than 40). However, detailed three-dimensional mapping by Ulery and Updike (1984) and Updike (1986) has shown that these high sensitivity soils occur as distinct sedimentary layers which coincide with the inferred zones of failure of the 1964 landslides. The fabric of sensitive clays in the Bootlegger Cove Formation has informally been postulated to be a flocculated open framework

of clay-size particles with water filling the abundant void spaces of the fabric. When sheared this fabric presumably collapses to a dispersed condition in which the platy clay particles re-orient subparallel to each other, the weight of the soil structure is carried by the pore water, and "quick" conditions result. The horizontal shear stresses of a large-magnitude earthquake are sufficient to cause the collapse, and, if the earthquake is of sufficient duration, the strength loss in this layer can cause the overlying sediments to be displaced laterally in the direction of least resistance (e.g., a bluff face). Recent field and laboratory testing (Updike, 1983, 1984; Idriss, 1985; Updike and Carpenter, 1986) firmly supports sensitive clay failure as the triggering cause of the major landslides in the Anchorage area.

The intent of the investigation reported here is to examine the microfabrics of the Bootlegger Cove Formation using the scanning electron microscope (SEM). The high magnification and resolution, as well as the three-dimensional character of the image viewed, allow for the best available method for microfabric study.

In 1982, an elaborate geotechnical investigation of a proposed high-rise state office building site was conducted in and adjacent to the 4th Avenue landslide zone. The atypically rigorous scope of the investigation was particularly focused toward the seismic hazard issue. The results of the geotechnical work (Idriss and Moriwaki, 1982) have not yet been formally published. As part of that effort, numerous undisturbed samples were required for advanced laboratory testing. The sample cores were acquired using a thin-walled piston sampler (length = 76.0 cm; diameter = 7.5 cm

O.D.). Several of these samples were not utilized in the testing program and, instead, were provided to the authors.

In addition to the downtown Anchorage site, three undisturbed cores from Lynn Ary Park, adjacent to the Turnagain Heights landslide, were provided by the U.S. Geological Survey for this study. Lynn Ary Park has been the site of several recent geotechnical cooperative investigations between the USGS and ADGGS. Similar stratigraphic sequences and physical states exist at the two sites.

Engineering geologic facies of the Bootlegger Cove Formation

Researchers generally agree that the Bootlegger Cove Formation was deposited during late Naptowne (late Wisconsinan) time (Reger and Updike, 1983). The formation was formerly named the "Bootlegger Cove Clay" and defined primarily on the basis of the cohesive units (Miller and Dobrovolny, 1959) as a light gray, silty clay, locally called the "blue clay". The type locality for the clay is at Bootlegger Cove, east of the 1964 Turnagain Heights landslide. The unit has been renamed because clay commonly is a secondary constituent, and the unit has been expanded to encompass a variety of sediment textures ranging in size from clay to boulders. The formal nomenclature "Bootlegger Cove Formation" has been chosen (Updike and others, 1982; Updike and Carpenter, 1986) because it is consistent with the stratigraphic code where two or more rock types are common. The diversity of textures results from a variety of depositional regimes tied to a glaciomarine-glaciodeltaic system. Seven geologic facies are defined based upon their engineering and textural parameters, each reflecting the subtle variations characteristic of a late Pleistocene glaciomarine environment:

Facies F.I	CLAY, with very minor silt and sand
Facies F.II	SILTY CLAY AND/OR CLAYEY SILT
Facies F.III	SILTY CLAY AND/OR CLAYEY SILT, sensitive
Facies F.IV	SILTY CLAY AND/OR CLAYEY SILT, with thin silt and sand lenses
Facies F.V	SILTY CLAY AND/OR CLAYEY SILT, with random pebbles, cobbles, and boulders
Facies F.VI	SILTY FINE SAND, with silt and clay layers
Facies F.VII	FINE TO MEDIUM SAND, with traces of silt and gravel

Recent three-dimensional regional mapping has emphasized the geologic and engineering implications associated with these facies (Updike, 1982, 1986; Ulery and Updike, 1984).

At the maximum extent of the late Naptowne glacial advance (Late Wisconsinan) (Reger and Updike, 1983), an ice front entered the Anchorage basin from the north, terminating west of the present Anchorage land area (fig. 2). The Anchorage area is believed to have also been glacially bounded to the northeast by the Knik-Matanuska glacial lobe and to the south by the Turnagain glacial lobe, creating an environment that at times limited the influx of marine water from lower Cook Inlet, and resulted in fluctuations between marine and brackish-fresh waters. Ablation of the northwest ice terminus produced a glacial fan delta prograding eastward into the deeper waters of the basin. The non-cohesive facies F.VI and F.VII extend eastward from this ice front. They are found to grade into and be interbedded with the cohesive facies F.I through F.V, representing transitions from the coarser deltaic regime into the finer deep-water regime. Although

fluctuations of the fan delta are evident from observed interbedding of the facies, this textural sequence generally reflects the gradational nature of the system from glaciodeltaic to a deep water regime. The glaciodeltaic deposition continued to be active throughout the period in which an ice front existed to the west. Generally, the non-cohesive facies (F.VI and F.VII) are the dominant units in the west, and the cohesive facies of the traditional "Bootlegger Cove Clay" (F.I through F.V) are most abundant in the east. The 1964 landslides have been attributed to liquefaction and/or sensitive clayey silt failures respectively associated with facies F.VI and F.III.

Most of the Bootlegger Cove sequence is capped by very fine to coarse, well-sorted sand beds (facies F.VI and F.VII) that represent the waning phase of the Bootlegger Cove Basin after the source-area ice had stagnated, glacial dams had been breached, and the basin was essentially drained. These sands at the top of the formation are typical throughout Anchorage, regardless of the overlying stratigraphy, implying that little erosion of the upper surface has occurred since their deposition in Late Pleistocene time (about 12,500 yr B.P.).

Method of Investigation

The piston sampler cores were extruded using an hydraulic ram. Descriptive logs were made of each core, representative segments were utilized for index property tests (including moisture content, density, Atterberg limits, penetrometer, Torvane, laboratory vane, unconfined compression, and hydrometer analyses); and key samples were identified for the scanning electron microscopy. These latter samples were double sealed in

cheese cloth and wax. The samples were then hand-carried from Alaska to the USGS laboratories in Menlo Park.

A critical aspect in the examination of the microfabric of intact samples of silt and clay soils is the method of drying. Because the SEM procedure requires 100 percent dry samples, it is necessary to extract all interstitial water. Standard methods of drying (e.g., air drying, oven drying, and microwave) can cause the fabric to shrink or otherwise be disrupted. Therefore, a recently developed technique, critical point drying, (Bennett and others, 1977; Schwab and Torresan, personal communication, 1984) was selected. This method of dehydration involves a sequential replacement of the water by Freon 13. The surface tension problems associated with change of state (liquid to gas) of soil water are essentially eliminated using Freon 13 because of the total and nearly-instantaneous "liquid to gas" phase change at a critical temperature of 28.9°C and a pressure of 39.27 kg/cm^2 (561 psi). The critical point drying was executed in the USGS Branch of Pacific Marine Geology, Marine Sediment Laboratory.

As each core sample was opened from the wax-cloth seal in the laboratory, samples were cut from the centers of each core using a fine wire knife. These subsamples were about 1.5 cm^2 cubes, each carrying a notation of the original orientation of each cube in the core. The samples were then wrapped in lens tissue for ease of handling and to prevent contamination. The samples were initially submerged in distilled water. Subsequently, in 30-minute time intervals, each sample was immersed in varying concentrations of anhydrous denatured ethyl alcohol ranging from a 10-percent solution to 100-percent alcohol, in 10-percent increments of increasing concentration.

Once 100-percent ethyl alcohol saturation was attained, the samples were allowed to remain in this fluid for at least 12 hrs, in airtight glass containers.

After the water to alcohol replacement was completed, a similar set of interstitial fluid replacements from alcohol to Freon TF fluorocarbon solvent (trichlorotrifluoroethane) was executed, beginning with 90-percent alcohol 10-percent Freon TF, and concluding with immersion in a 100-percent Freon TF solution. Each immersion was maintained for 30 minutes, with the final immersion at 100-percent concentration being repeated and allowed to stand for 12 hours.

The final fluid exchange from Freon TF to Freon 13 (monochlorotrifluoromethane) was accomplished in the Ladd Critical Point drying apparatus (fig. 3). This is a pressure-temperature bomb into which the Freon TF-saturated samples were introduced and sealed. The drying chamber was flooded with Freon 13 and the samples allowed to soak for 15 minutes. The chamber was drained and then refilled with Freon 13. With the transitional fluid replacement completed, temperature and pressure were elevated to and above the critical point for Freon 13. The system was held at 40°C for approximately 15 minutes, then a drain was partially opened to allow Freon 13 gas to be slowly tapped off. While maintaining the elevated temperature, all of the gas was thus evacuated from the chamber and totally dried samples resulted.

Using a razor blade, the dried samples were fractured along selected planes and then mounted on standard SEM stubs using silver paint as an

adhesive (fig. 4). Each sample was electrostatically cleaned to remove loose debris using the technique of Hulbert and Bennett (1975). The samples were then coated with gold-palladium in a Technics Hummer vacuum sputter coater for 5 minutes to provide a conductive surface for the SEM. A total of 73 stubs were thus produced from the two field localities.

The Cambridge Stereoscan 180 scanning electron microscope at the Office of the Chief Geologist, USGS, Menlo Park, California, was used for all examinations and photography (fig. 5). The system is interfaced with the energy dispersive X-ray analyzer (Edax 707B) which allows spot-checking of mineral grain composition within the plane of view (fig. 6).

Results

Systematic examination of all stub samples was made by the authors, with 134 Polaroid photographic images being made of typical fabrics as well as specific features. Of these, 42 selected images are illustrated in figures 7 to 48.

The primary objective of this report is to provide a catalog of images representative of the variety of fabrics observed. Specific results and interpretations from this work will be reported elsewhere. However, some general conclusions are outlined below.

1. Each of the engineering geologic facies of the Bootlegger Cove Formation (which have previously been defined on the basis of geologic and engineering parameters) is clearly distinctive at the microfabric scale.

However, locally within certain facies, sample features typical of other facies were occasionally observed.

2. Whereas the silt and fine sand grains have a spherical to prismoidal form, the clay size grains are generally platy. There is, however, no general difference in mineralogy between these different grain sizes.

3. The bedding planes of all facies were clearly distinguishable at the microscopic level, by the arrangement of clay and silt grains.

4. Facies F.I and F.II are dominantly clay-size sediments with a subparallel arrangement of the clay grains commonly having their minimum axes normal to sample bedding. Silt grains variously occur randomly dispersed, as distinct packets, or as 1 to 3 grain thick continuous layers.

5. The sensitive facies (F.III) is predominantly clay-size sediment with silt grains usually randomly dispersed throughout. The fabric has a framework which varies from partially compressed to open flocculated (boxwork or "house-of-cards"), to a honey-comb structure (Collins and McGown, 1974)(e.g., figs. 24 and 28). In most instances the fabric is metastable, that is, edge-to-edge and edge-to-face associations between grains are typical. This implies that the particles flocculated during sedimentation and, in the subsequent 14,000 years, the fabric has been able to carry the effective stresses imposed without significant compression. A recent discussion of this mechanism is given by Torrance (1983).

6. In addition to maintaining the static load, much of the fabric has seemingly remained unaffected by occasional seismic loading events. At many locations within representative views, collapsed clay zones were noted. These "failure" zones bounded the metastable regions as compoundly-curved planes a few clay grains thick (e.g., figs. 33 - 32). The visual implication is that the resultant strain has been taken up along discrete planes with the adjacent soil remaining intact. It is not possible to determine whether these collapse zones are due to static or dynamic stresses.

7. Close examination at the magnification limits of the SEM (22,000X) resulted in no evidence to suggest cementation at grain boundary contacts to be a significant fabric binder in any of the cohesive soil facies (fig. 32), and only rarely in F.VI (fig. 48).

8. Facies F.IV and F.V varied in the relative abundance of clay and silt. Stratification was usually evident both in the alternation of silt and clay bands, and the sinuous, collapsed (turbostratic) character of the clay layers. Compact, dispersed clay aggregates commonly serve as binding connectors between silt grains. In F.IV, sample porosity is related to inter-particle, inter-assemblage, and intra-assemblage pores. The fabric of F.V, on the contrary, is much more highly compressed resulting in a higher degree of infilling of silt interparticle pores with clay and a reduction in size and number of intra-assemblage pores. This causes a pronounced increase in soil strength due to tighter packing and inter-particle rigidity. Facies F.V is unique from the other cohesive facies in that the clay aggregations form casts around

the silt grains (figs. 42 and 43). This could be caused by excessive prehistoric loading (for example, by ice) or by shrinkage due to desiccation.

9. The coarse, non-cohesive character of facies F.VII causes it to be outside the capabilities of this study. A few samples of F.VI were successfully prepared and examined (figs. 44 through 47). Where clays were present they served as connectors between the silt and fine sand grains. Some iron oxide precipitates were noted between and coating the grains, but both clay connectors and precipitates were often nearly absent. Moderate to dense packing apparently accounts for the observed high penetration resistance (e.g., see Updike, 1984).

Conclusions

Because of the seismic ground failure hazard associated with the Bootlegger Cove Formation, numerous research-oriented and applied geotechnical studies have evaluated the Formation during the past 20 years. Predictions and hypotheses on the fabric have abounded in the reports resultant from these studies. Herein, for the first time, a systematic examination of the engineering geologic facies fabrics is provided through use of careful sample preparation and scanning electron microscopy. The dramatic difference in the fabric of the sensitive facies compared to the other facies serves to emphasize the fragility of that facies and the capacity of the formation to fail again in future earthquakes. The presence of the sensitive facies throughout much of central and western Anchorage emphasizes the need for conscientious engineering design to mitigate the potential failure of these soils.

Future studies utilizing the techniques described above should include "before-and-after" examination of facies fabrics associated with samples subjected to laboratory testing (e.g., cyclic triaxial, resonant column, static triaxial, consolidation). In addition, the in situ fabrics should be compared to representative samples from 1964 landslides and from late Holocene sediment analogs in glacio-lacustrine basins and the Gulf of Alaska.

Acknowledgements

This work was partially supported by USGS Agreement 14-08-0001-A-0026 under the Earthquake Hazards Reduction Program and by operational funds of the Alaska Division of Geological and Geophysical Surveys. The Alaska Department of Transportation and Public Facilities (ADOT-PF) provided their materials laboratories for initial extrusion and index property testing. Thomas Moses, ADOT-PF State Soils Engineer, was very helpful in aquiring the samples. The authors are particualrly indebted to Bill Schwab, USGS-Woods Hole, and Mike Torresan, USGS-Menlo Park, and the Branch of Pacific Marine Geology for providing their expertise and laboratory facilities for the critical point drying technique. The scanning electron microscope laboratory at the U.S. Geological Survey offices in Menlo Park, California, was used for the fabric studies. The manuscript benefitted from the critical reviews of Robert Brown and Homa Lee, USGS-Menlo Park.

Glossary

Aggregation: The face-to-face association of several clay-size particles (Van Olphen, 1963).

Assemblage: Units of particle organization having definable physical boundaries and a specific mechanical function (Mitchell, 1976).

Cardhouse (or boxwork): An edge-to-face arrangement of clay platelets forming an open fabric (Goldschmidt, 1926).

Clay: (a) as a particle size term, usually refers to grains smaller than 2 um; (b) as a mineral term, refers to a group of hydrous aluminum silicates, usually occurring as platy crystalline aggregates. Note: not all clay minerals occur as crystals less than 2 um and not all clay-size particles are clay minerals.

Cohesive soil: The mass property of a fine-grained soil in which particles of similar or differing compositions cohere due to surface forces, cementation, capillary stresses, or apparent mechanical forces.

Colloid: A particle size less than clay-size particles, i.e., less than 0.24 um.

Connector: A generally compact unit of clay-size particles which forms a bridge-like connection between two assemblages, or two silt or sand-size grains.

Dispersed: An arrangement of clay particles in which no face-to-face association of clay particles exists (Van Olphen, 1963).

Effective stress: The total stress exerted on a plane of a soil element minus the pore-water pressure; this stress in turn controls certain aspects of soil behavior, such as liquefaction.

Fabric, soil: The physical arrangement of the soil particles including the particle spacing and pore size distribution. Macrofabric can be observed with the naked eye or hand lens; microfabric requires microscope magnification (Collins and McGown, 1974).

Facies, engineering geologic: A sedimentary unit (soils unit) possessing the characteristics of a geologic facies, but in addition, defined on the basis of engineering soils criteria that are dictated by the geologic history and ambient conditions of the unit (Updike and Carpenter, 1986).

Flocculated: Edge-to-edge or edge-to-face association of clay size particles (Van Olphen, 1963) or aggregates (Collins and McGown, 1974).

Glaciodeltaic: Sedimentation of glacially-derived materials generally transported by streams issuing from the terminus of a glacier into a water body, resulting in sedimentary features characteristic of a fluvial delta.

Glaciomarine: Sedimentation of glacially-derived materials in a marine environment, usually directly beyond the terminus of a glacier fronting on the ocean.

Honeycomb structure: The arrangement wherein individual clay-size particles interact and form open networks surrounding large regular voids (Collins and McGown, 1974).

Metastable fabric: The initial fabric after flocculated sedimentation involving some amount of edge-to-edge and edge-to-face associations and which, during consolidation, carries a higher effective stress than would be possible in a parallel array (Mitchell, 1976).

Sensitive clay: A soil consisting predominantly of clay-size particles which are arranged in a fabric which shows measurable undrained strength loss when remolded.

Turbostratic: Here refers to assemblage or fabric in which there is a turbulent array of fabric units consisting of parallel oriented clay platelets (Aylmore and Quirk, 1960).

Void: The pore spaces occurring between individual particles or assemblages. Intra-assemblage voids occur within an assemblage; inter-assemblage voids occur between assemblages.

References Cited

Aylmore, L.A.G., and Quirk, J.P., 1960, Domain or turbostratic structure in clays: Nature, v. 187, p. 1046.

Bennet, M.J., Youd, T.L., Harp, E.L., and Wieczorek, G.F., 1981, Subsurface investigation of liquefaction, Imperial Valley Earthquake, California, October 15, 1979: U.S. Geological Survey Open-File Report 81-502, 83 p.

Bennett, R.H., Bryant, W.R., and Keller, G.H., 1977, Clay fabric and geotechnical properties of selected submarine sediment cores from the Mississippi Delta: NOAA Professional Paper No. 9, U.S. Department of Commerce NOAA-ERC Publication, 86 p.

Collins, K., and McGown, A., 1974, The form and function of microfabric features in a variety of natural soils: Geotechnique, V. 24, No. 2, pp. 223-254.

Goldschmidt, V.M., 1926, Undersokelser over lersedimenter: Nordisk jordrugsforskning, Nos. 4-7, p. 434-445.

Hansen, W.R., 1965, Effects of the earthquake of March 27, 1964, at Anchorage, Alaska: U.S. Geological Survey Professional Paper 542A, pp. A1-A68.

Hulbert, M.H., and Bennett, R.H., 1975, Electrostatic cleaning techniques for fabric SEM samples: Clays and Clay Minerals, V. 23, p. 33.

Idriss, I.M., 1985, Evaluating seismic risk in engineering practice: XI International Conference on Soil Mechanics and Foundation Engineering, San Francisco, Theme Paper, 66 p.

Idriss, I.M., and Moriwaki, Y., 1982, Anchorage Office Complex geotechnical investigation, Anchorage, Alaska, Vol. 1, Seismic hazards evaluation: San Francisco, Woodward-Clyde Consultants, pp. 6-1 to 6-3.

Kerr, P.F., and Drew, I.M., 1965, Quick clay movements, Anchorage, Alaska: Springfield, Virginia, National Technical Information Service, Doc. AD630-111, 133 p.

Miller, R.D., and Dobrovolny, Ernest, 1959, Surficial geology of Anchorage and vicinity, Alaska: U.S. Geological Survey Bulletin 1093, 128 p.

Mitchell, J.K, 1976, Fundamentals of soil behavior: New York, John Wiley and Sons, 422 p.

Mitchell, J.K., Houston, W.N., and Yamane, G., 1973, Sensitivity and geotechnical properties of Bootlegger Cove Clay: National Academy of Sciences, The Great Alaska Earthquake of 1964 -- Engineering, p. 157-178.

Reger, R.D., and Updike, R.G., 1983, Upper Cook Inlet region and the Matanuska Valley in Pėwė, T.L. and Reger, R.D., Richardson and Glenn Highways -- Guidebook to permafrost and Quaternary Geology: Alaska Division of Geological and Geophysical Surveys, Guidebook 1, pp. 185-263.

Seed, H.B., 1968, Landslides during earthquakes due to soil liquefaction: Journal of Soil Mechanics and Foundations Division, American Society of Civil Engineers, V. 94, pp. 1053-1122.

_____, 1976, Evaluation of soil liquefaction effects on level ground during earthquakes: American Society of Civil Engineers Special Session on Liquefaction Problems in Geotechnical Engineering, Philadelphia, p. 1-104.

_____, 1979, Soil liquefaction and cyclic mobility evaluation for level ground during earthquakes: Journal of the Geotechnical Engineering Division, American Society of Civil Engineers v. 105, no. GT2 p. 201-255.

Seed, H.B., Idriss, I.M., and Arango, Ignacio, 1983, Evaluation of liquefaction potential using field performance data: Journal of Geotechnical Engineering, American Society of Civil Engineers, v. 109, p. 458-482.

Seed, H.B., and Wilson, S.D., 1967, The Turnagain Heights Landslide, Anchorage, Alaska: Journal of the Soil Mechanics and Foundations Division, American Society of Civil Engineers, V. 93, pp. 325-353.

Shannon and Wilson, Inc., 1964, Report on Anchorage area soil studies, Alaska, to the U.S. Army Engineer District, Anchorage, Alaska: Seattle, Washington, Shannon and Wilson, Inc., 109 p.

Torrance, J.K., 1983, Towards a general model of quick clay development: Sedimentology, V. 30, pp. 547-555.

Ulery, C.A., and Updike, R.G., 1984, Subsurface structure of the cohesive facies of the Bootlegger Cove Formation, southwest Anchorage, Alaska: Alaska Division of Geological and Geophysical Surveys Professional Report 84, 6 pp. and 3 map plates (1:15,840).

Updike, R.G., 1982, Engineering geologic facies of the Bootlegger Cove Formation, Anchorage, Alaska (Abstract): Geological Society of America 95th Annual Meeting, New Orleans, Abstracts with programs, p. 636.

_____1983, Seismic liquefaction potential in the Anchorage area, south-central Alaska (Abstract): Geological Society of America Symposium on the Engineering Geology of Liquefiable Deposits in the Western U.S., 1983 Cordilleran and Rocky Mountain Section Meeting, Salt Lake City, p. 374.

Updike, R.G., 1984, The Turnagain Heights Landslide--an assessment using the electric cone penetration test: Alaska Division of Geological and Geophysical Surveys Report of Investigation 84-13, 48 p.

_____, 1986, Engineering geologic maps of the Government Hill area, Anchorage, Alaska: U.S. Geological Survey Map I-1610, 1 sheet, 1:4800.

Updike, R.G., and Carpenter, B.A., 1986, Engineering geology of the Government Hill area, Anchorage, Alaska: U.S. Geological Survey Bulletin 1588, in press.

Updike, R.G., Cole, D.A., and Ulery, C.A., 1982, Shear moduli and damping ratios for the Bootlegger Cove Formation as determined by resonant-column testing, in Short Notes on Alaskan Geology-1981: Alaska Division of Geological and Geophysical Surveys Professional Report 73, p. 7-12.

Van Olphen, H., 1963, An introduction to clay colloid chemistry: New York, John Wiley and Sons, 301 p.

Youd, T.L., and Perkins, D.M., 1978, Mapping liquefaction-induced ground failure potential: Journal of Geotechnical Engineering Division, American Society of Civil Engineers, v. 104, GT4, p. 433-446.

Figure 1. Fourth Avenue landslide scarp immediately after March 27, 1964 Earthquake. View looking east toward intersection at 4th Avenue and "A" Street. Note approximately 3 m of vertical displacement. Sample locality for specimens used in this report approximately four blocks from this picture. (Photograph from NOAA-EDIS Files)

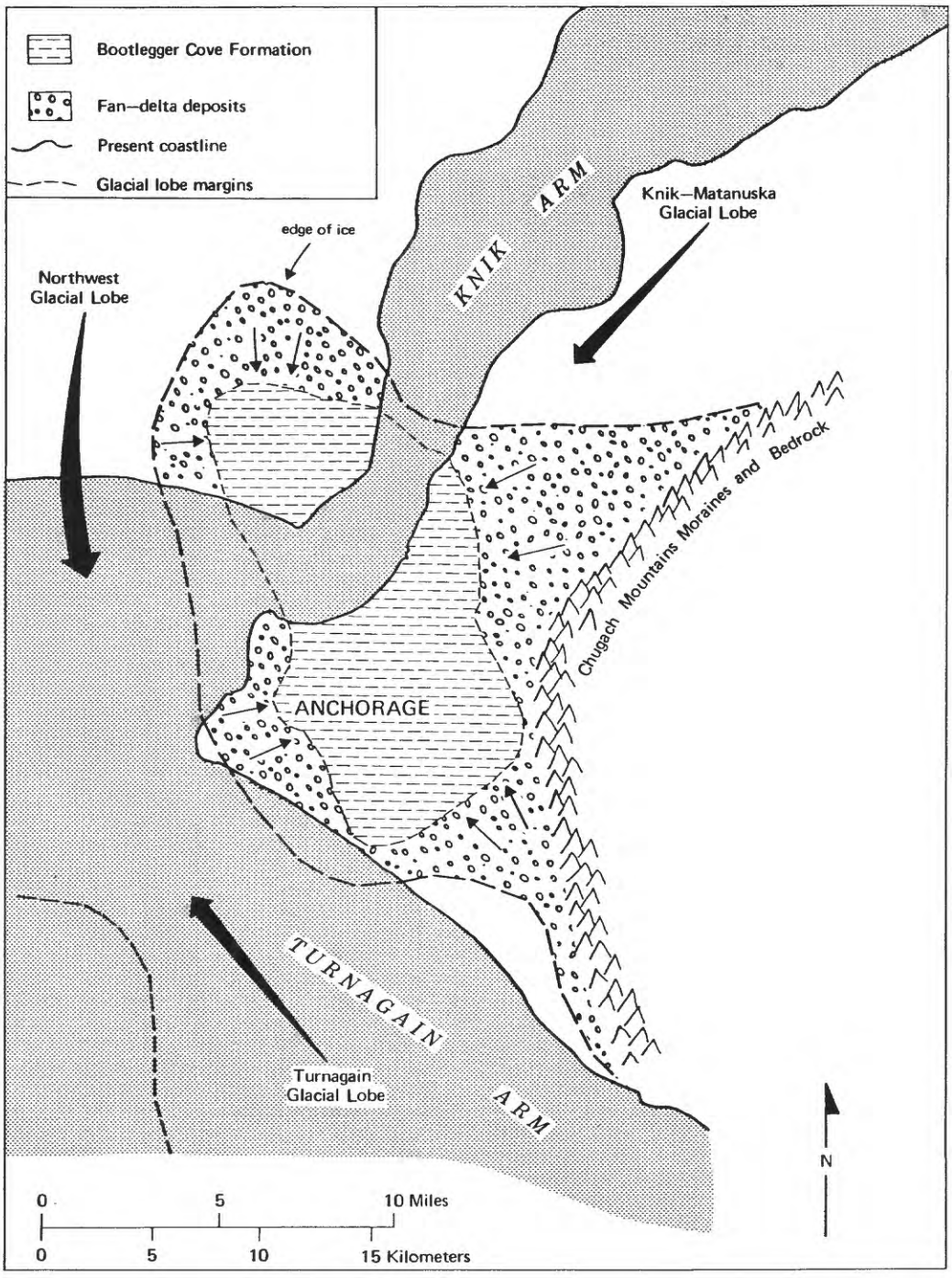

Figure 2. Idealized map showing the relationship of major glacial ice-lobes that surrounded the Bootlegger Cove Formation depositional basin at about 14,000 years ago. Bold arrows show the general direction of ice flow; light arrows indicate the depositional trends of sediment derived from these lobes into the basin. The fan delta deposits graded laterally into the finer deposits in the center of the basin.

Figure 3. Ladd Critical Point Dryer, a pressure-temperature bomb used for Freon 13 phase conversion. Note sample in chamber prior to sealing with faceplate in foreground.

Figure 4. Preparation of sample for SEM after critical point drying. Split sample (center) will be trimmed and mounted on an alloy stub (top center) using silver paint. Prepared stubs are stored in desiccator until being plated with gold and palladium.

Figure 5. Cambridge Stereoscan 180 Scanning Electron Microscope, U.S. Geological Survey, Menlo Park, California.

Figure 6. EDAX 707B energy dispersive X-ray analyzer used in routine composition analyses of mineral grains viewed by the linked SEM system.

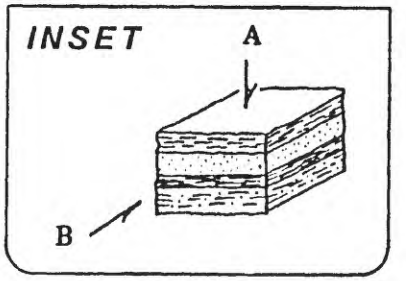

Figure 7. Orientation view; mag. = 3200X. Silt grain (s), clay grain (c), silt-clay assemblage (a), inter-assemblage void (rv), intra-assemblage void (av). Note clay grains clinging to the silt grains. Inset shows view orientation terminology used in the following figures. Dircetion "A" is a view normal to bedding planes; direction "B" is a view parallel to bedding planes.

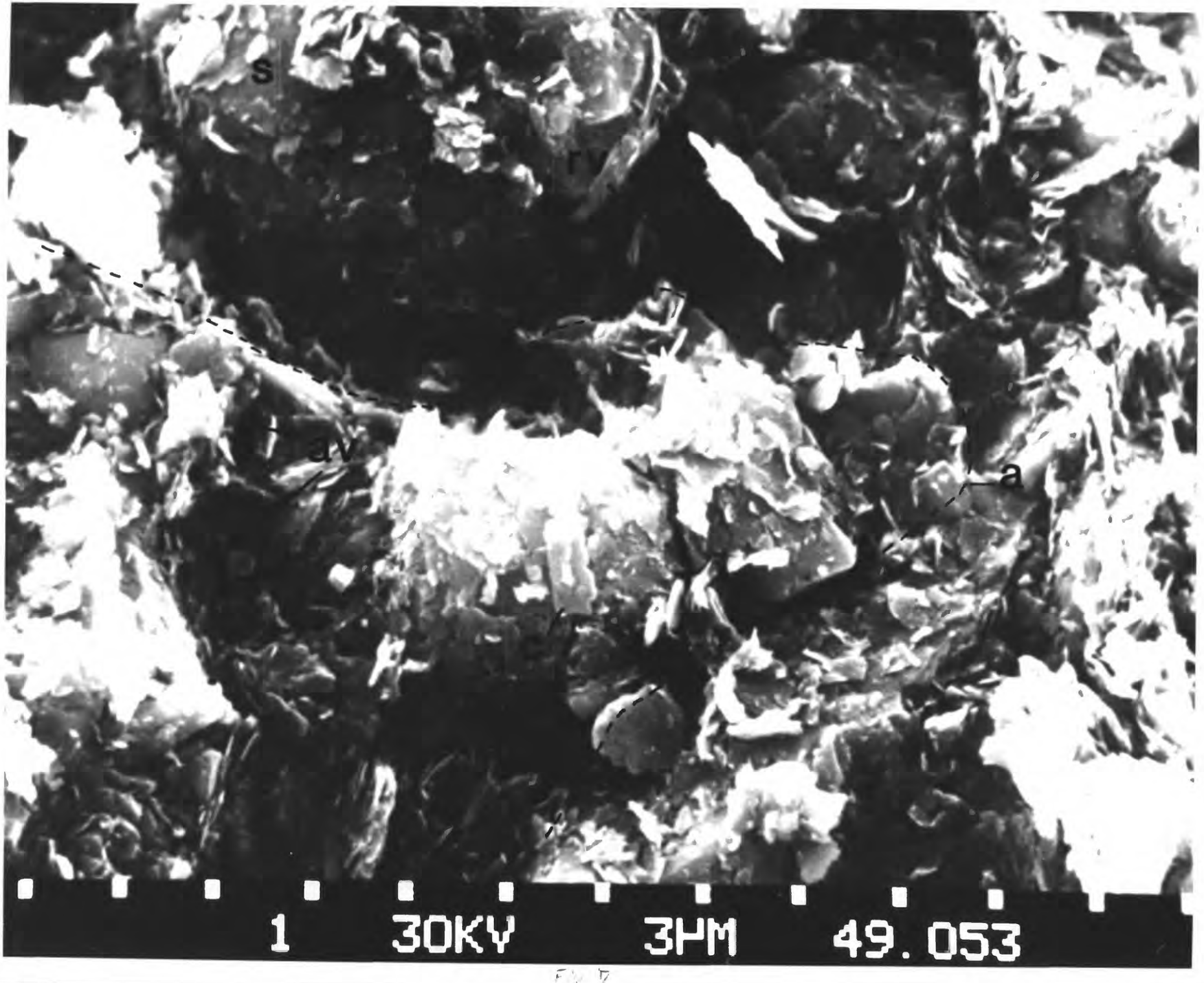
s
v
av
a
1 30KV 3PM 49.053

Figure 8. Facies F.III, parallel to bedding planes, mag. = 99X. Low magnification view of laminae shown at higher magnifications in figures 26 to 27.

20KV 300HM 49.064

Figure 9. Facies F.IV, parallel to bedding planes, mag. = 36X. Low magnification view of low sensitivity sample shown at high magnification in figure 42. Compare to high sensitivity sample having thinner laminae but otherwise similar appearance (fig.8).

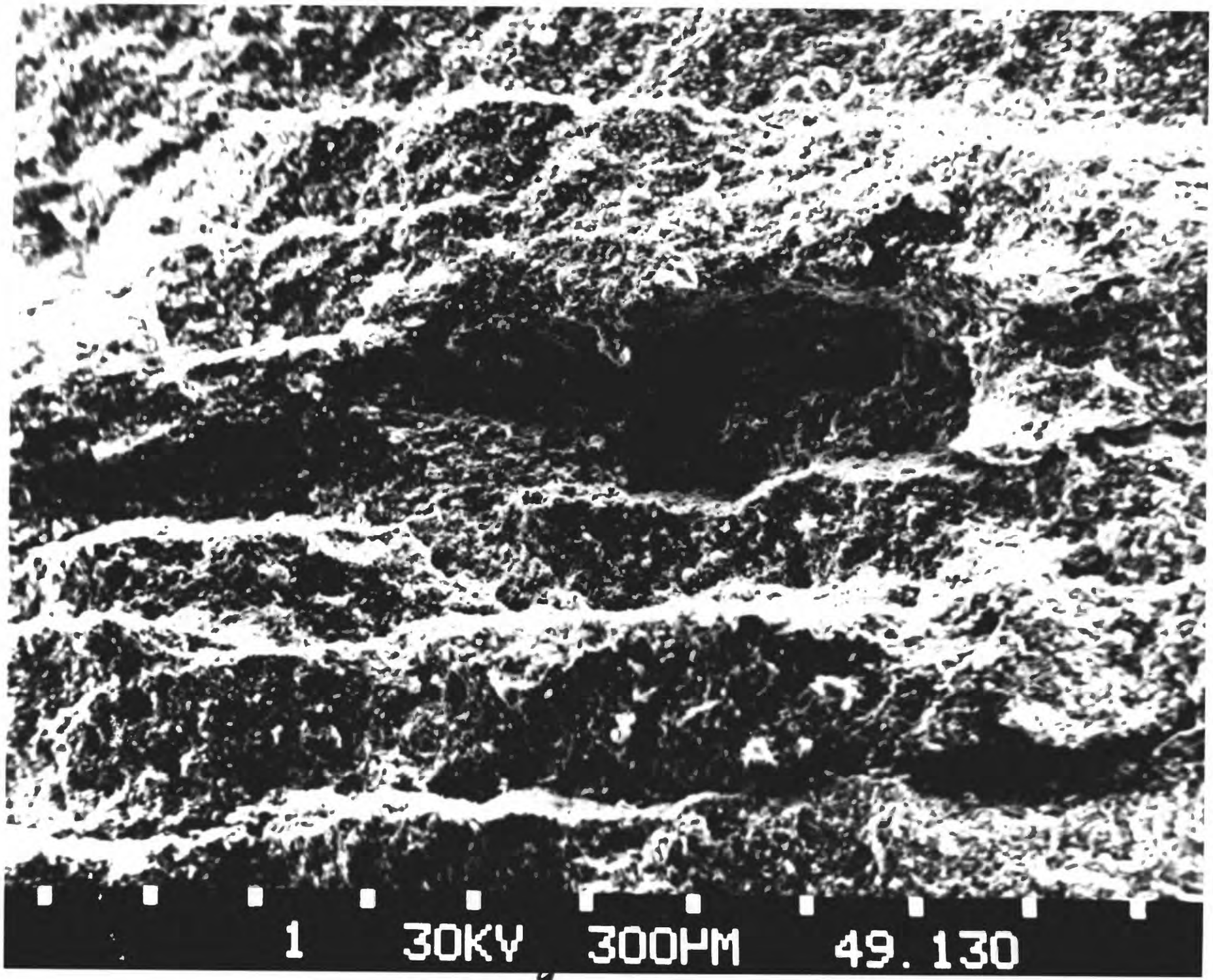
1 30KV 300UM 49.130

Figure 10. Facies F.I., parallel to bedding planes, mag. = 3600X. Dominantly clay-sized particles, rarely fine silt. Specimen from core varying from low to medium sensitivity. Note the elliptical intergranular voids.

1 30KV 3MM 49.000

Figure 11. Facies I, normal to bedding plane, mag. = 9900X. Essentially all clay-size particles, most lying in plane of bedding. Compare to figure 20. Note limited assemblage development due to uniformity of particle sizes and parallel orientation of grains.

1 30KV 1HM 49.051

Figure 12. Facies F.II, parallel to bedding planes, mag. = 3300X. Bedding strikes top to bottom. Clay platelets in turbostratic arrangement having more intra-assemblage porosity around silt grains. Contrast with figure 10. This sample generally yielded low sensitivity.

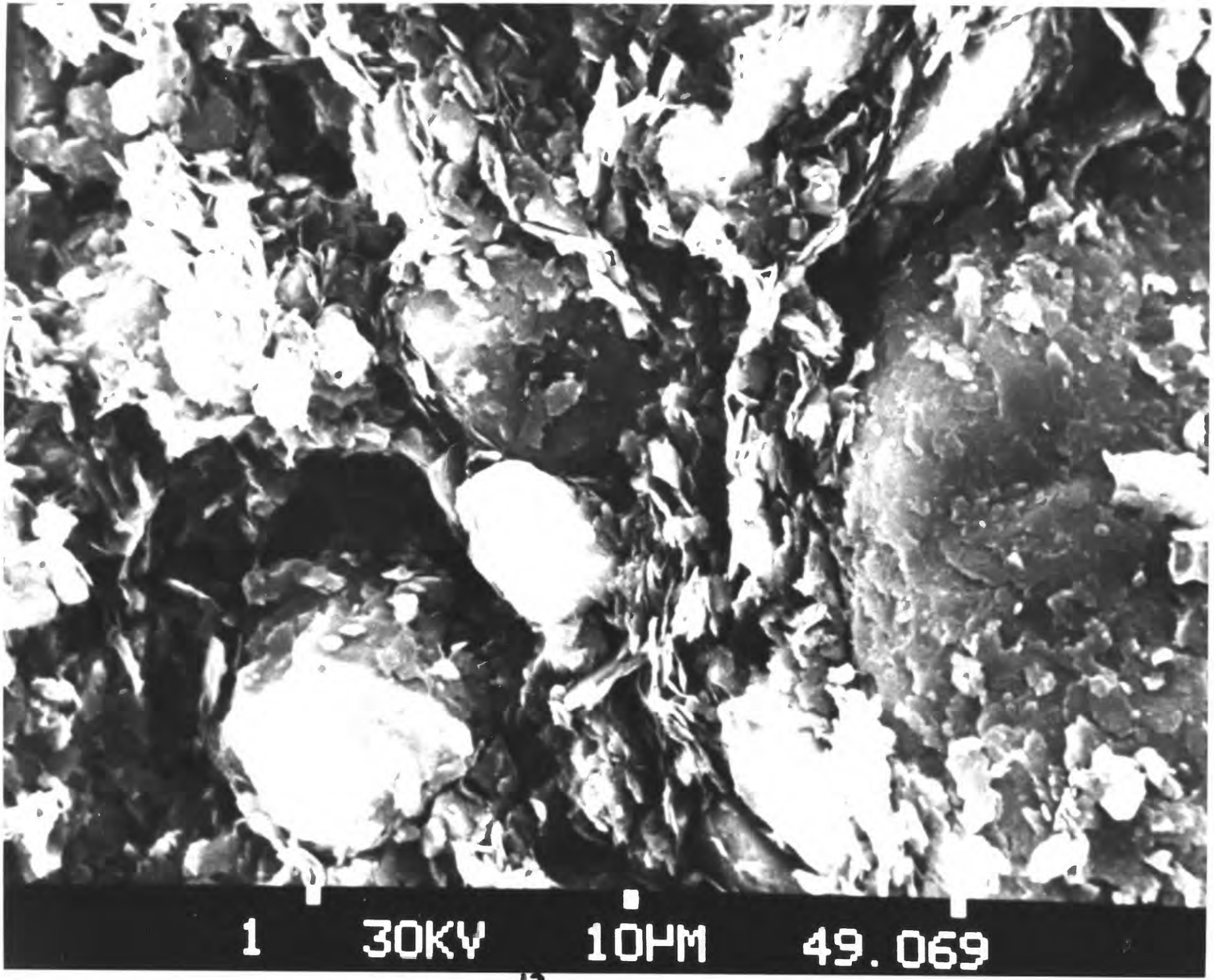
1 30KV 10UM 49.069

Figure 13. Facies F.II, parallel to bedding planes, mag. = 1010X. Bedding from upper left to lower right. Fully dispersed clay layers (df) interbedded with angular silt grains. Inter-assemblage voids (rv) predominate. Compare to partially flocculated fabric of figure 12.

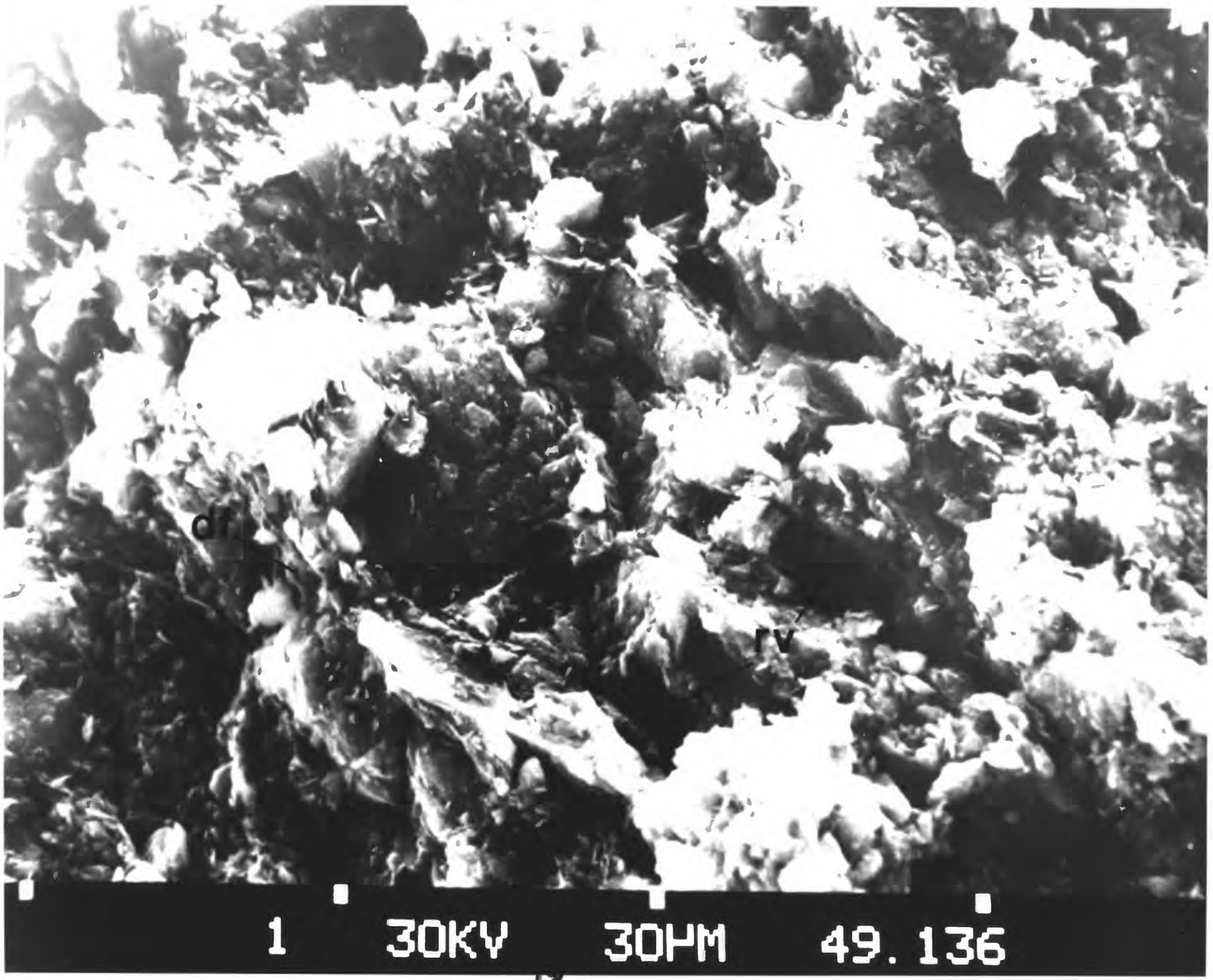
df
IV
1 30KV 30UM 49.136

Figure 14. Facies F.II, normal to bedding planes, mag. = 5700X. Both silt (s) and clay (c) oriented in bedding plane. Inter-assemblage voids (rv) small and indistinct.

b

Figure 15. Facies F.II, parallel to bedding planes, mag. = 3190X. Bedding from top to bottom, clay turbostratic groups (ts) with random scattered silt grains.

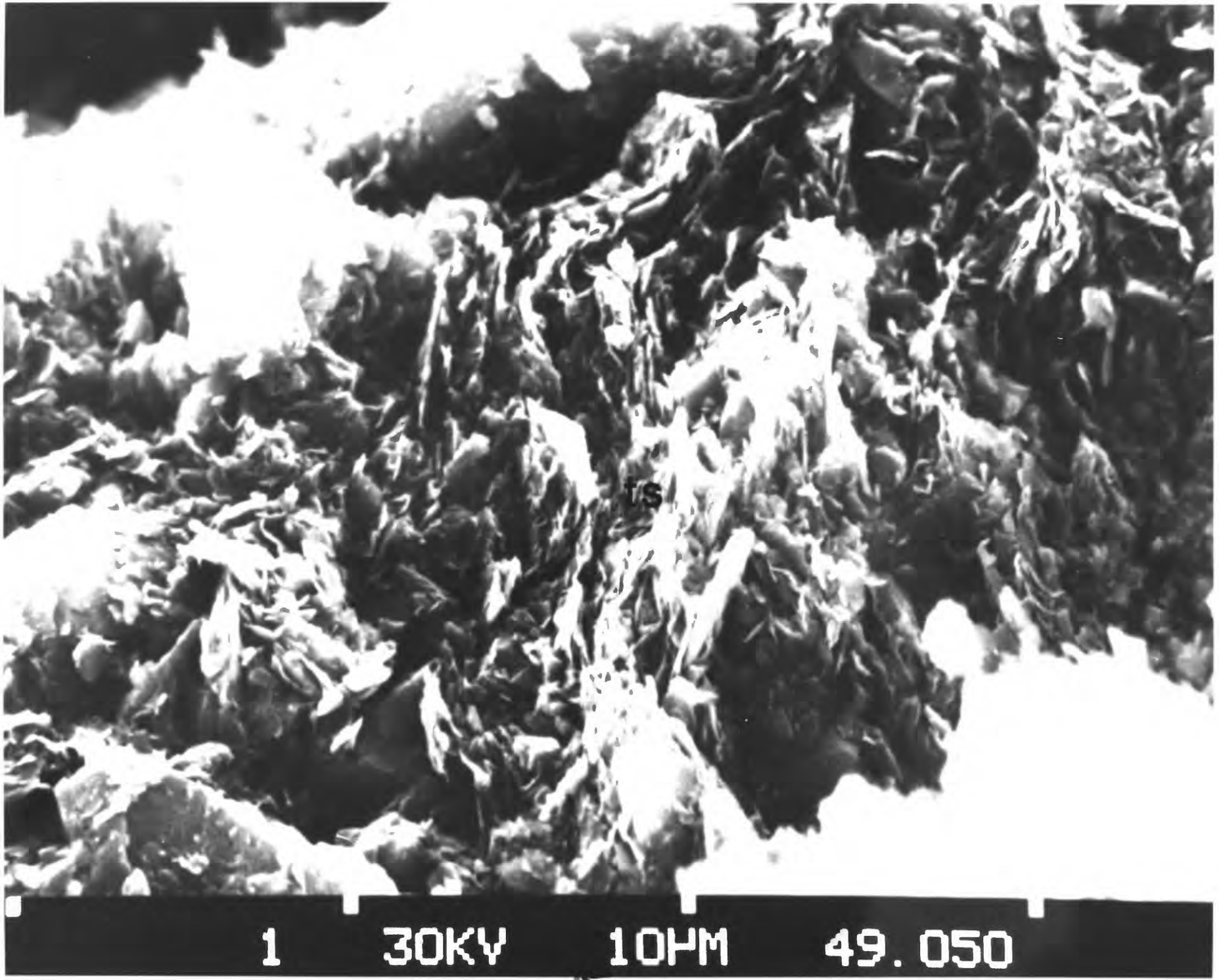
1 30KV 10UM 49.050

Figure 16. Facies F.II, normal to bedding, mag. = 10,000X. Detail along collapsed zone (cz) which has curvature suggesting shear strain may have occurred.

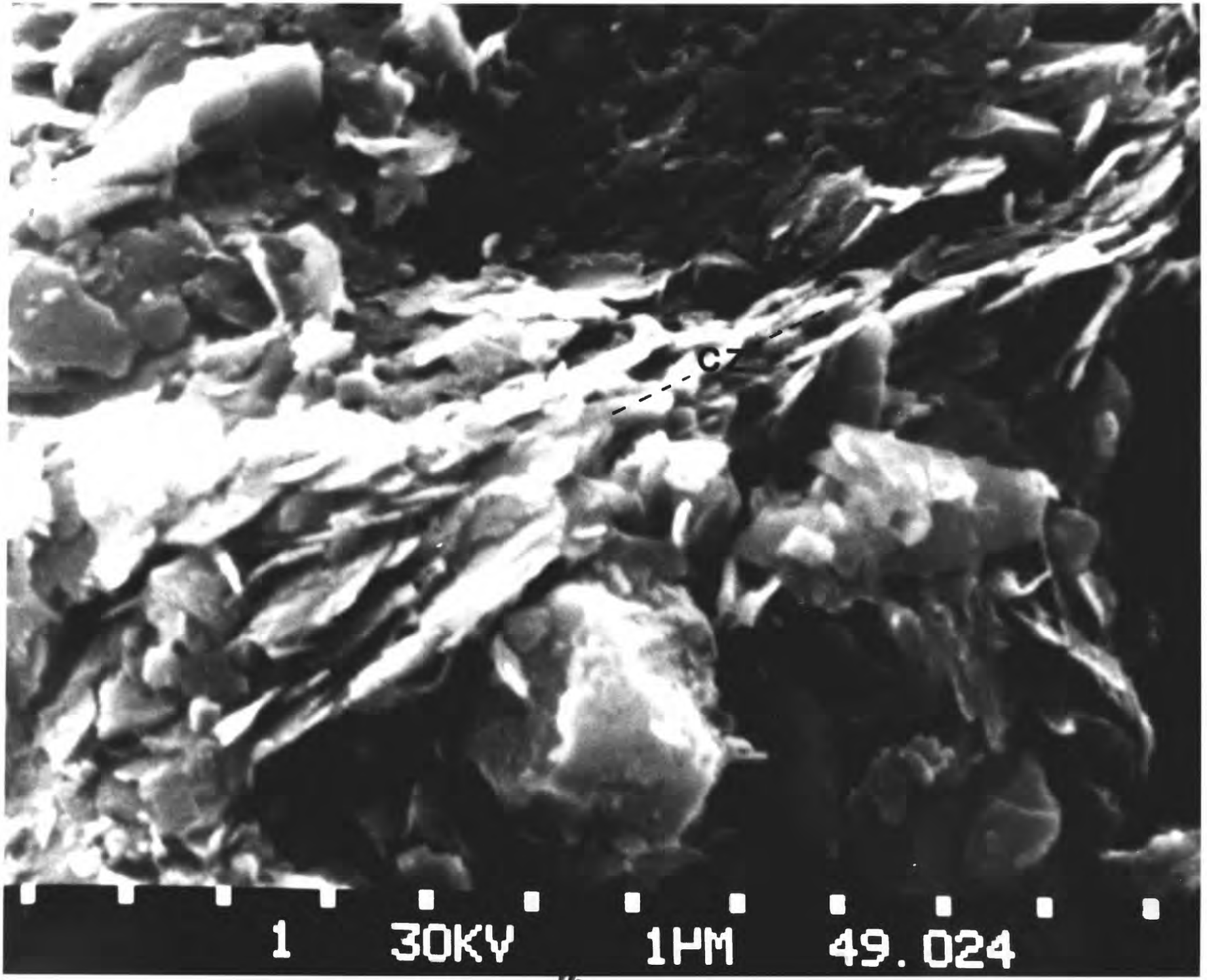
C
1 30KV 1PM 49.024

Figure 17. Facies F.II, parallel to bedding planes, mag. = 3700X. Approximately equal amounts of silt and clay, in laminae from left to right. Note distended eliptical voids in clay zones parallel to bedding.

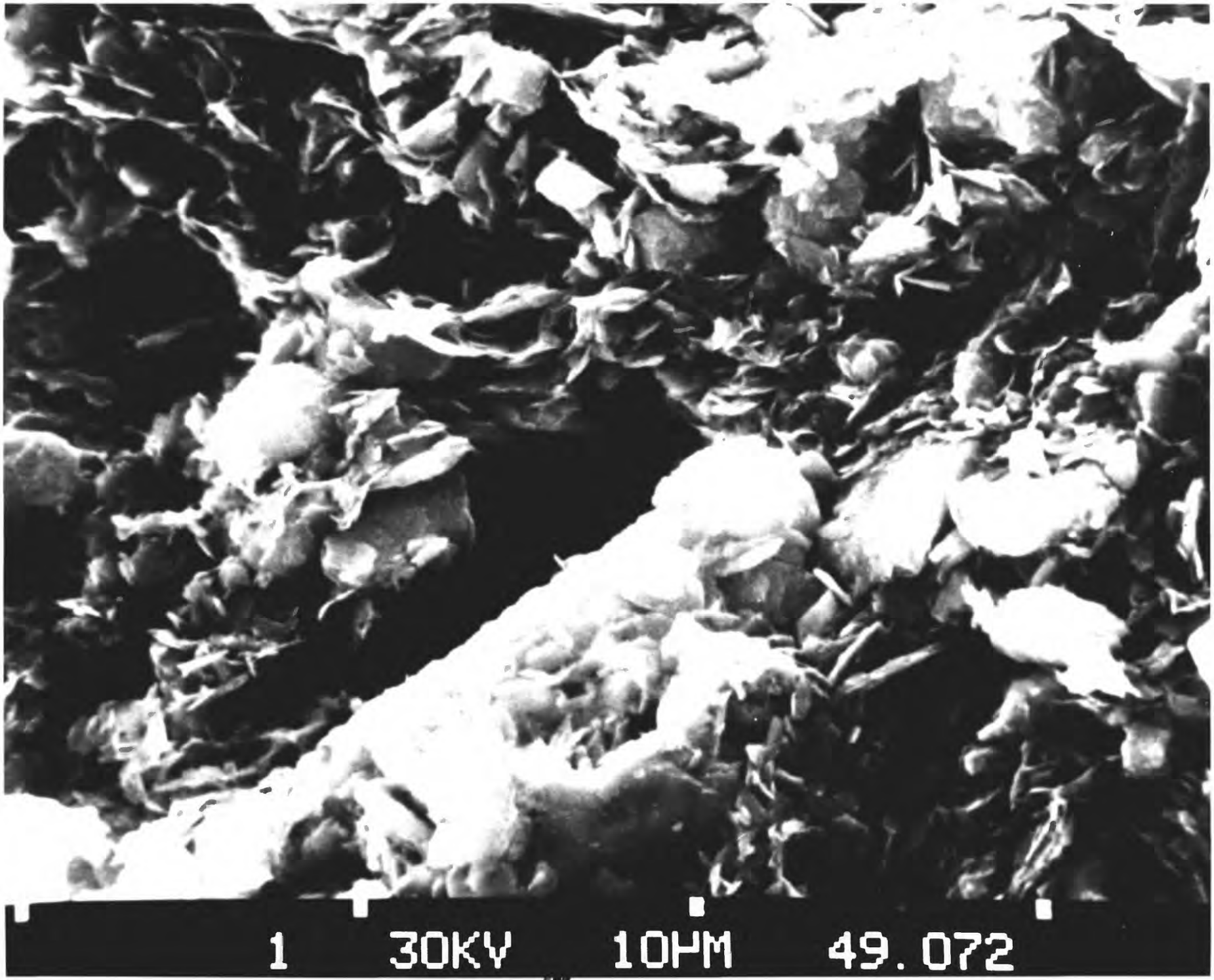
1 30KV 10UM 49.072

Figure 18. Facies F.II, normal to bedding, mag. = 2050X. This sample was medium sensitive although within F.II. Here flocculated fabric (of) is present but of restricted extent compared to figures 24 and 25. Colloidal floccules (cf) are also small and uncommon.

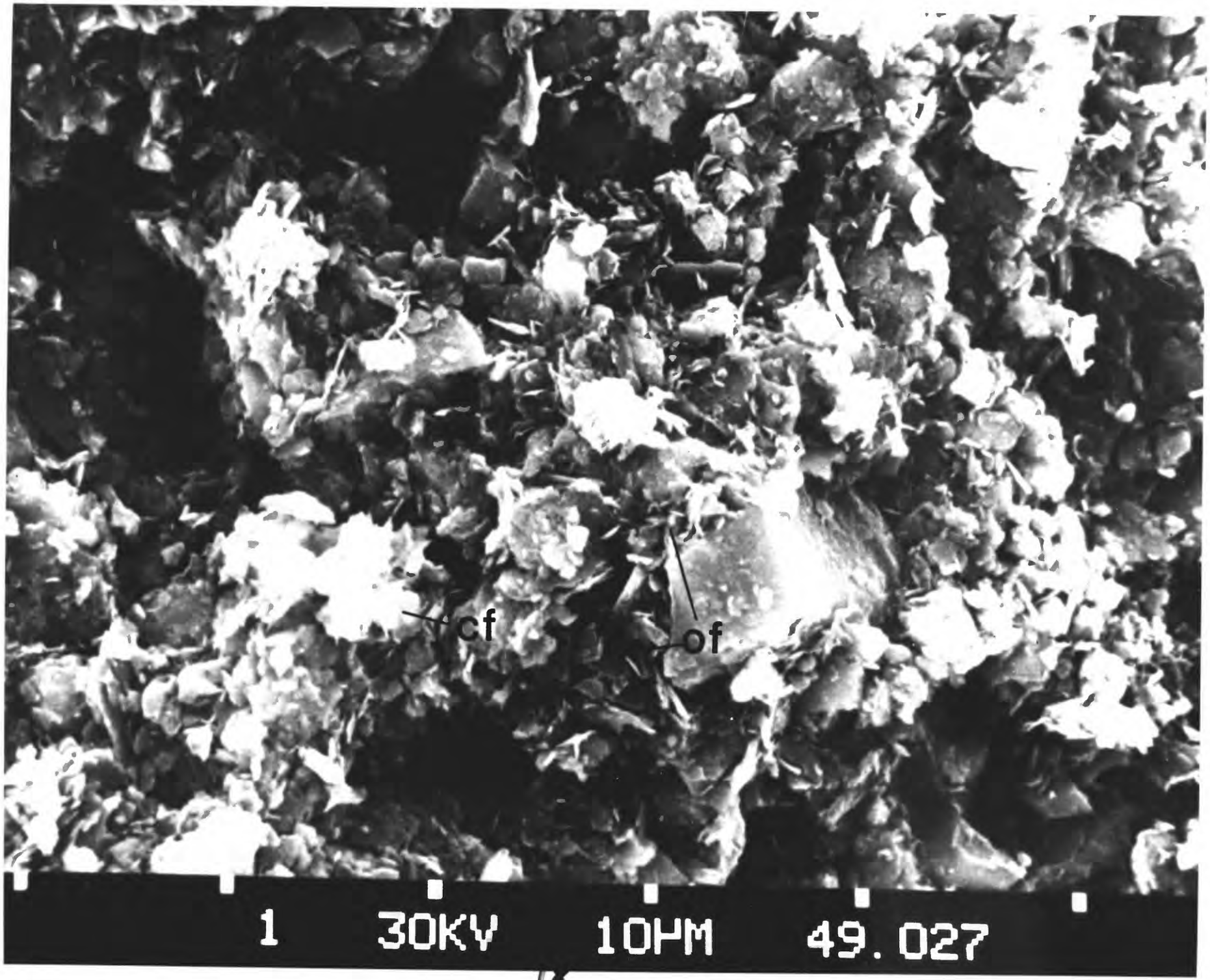
cf
of
1 30KV 10UM 49.027

Figure 19. Facies F.II, normal to bedding, mag. = 4200X. Fracture zone lower left to upper right. Silt common with clay as silt connectors. Silt grain weathering, presumably *in situ* (sw).

1 30KV 3MM 49.023
SWS

Figure 20. Facies F.III, normal to bedding planes, mag. = 4100X. Major axes of most of clay and silt grains in plane of image. See figures 21 and 22.

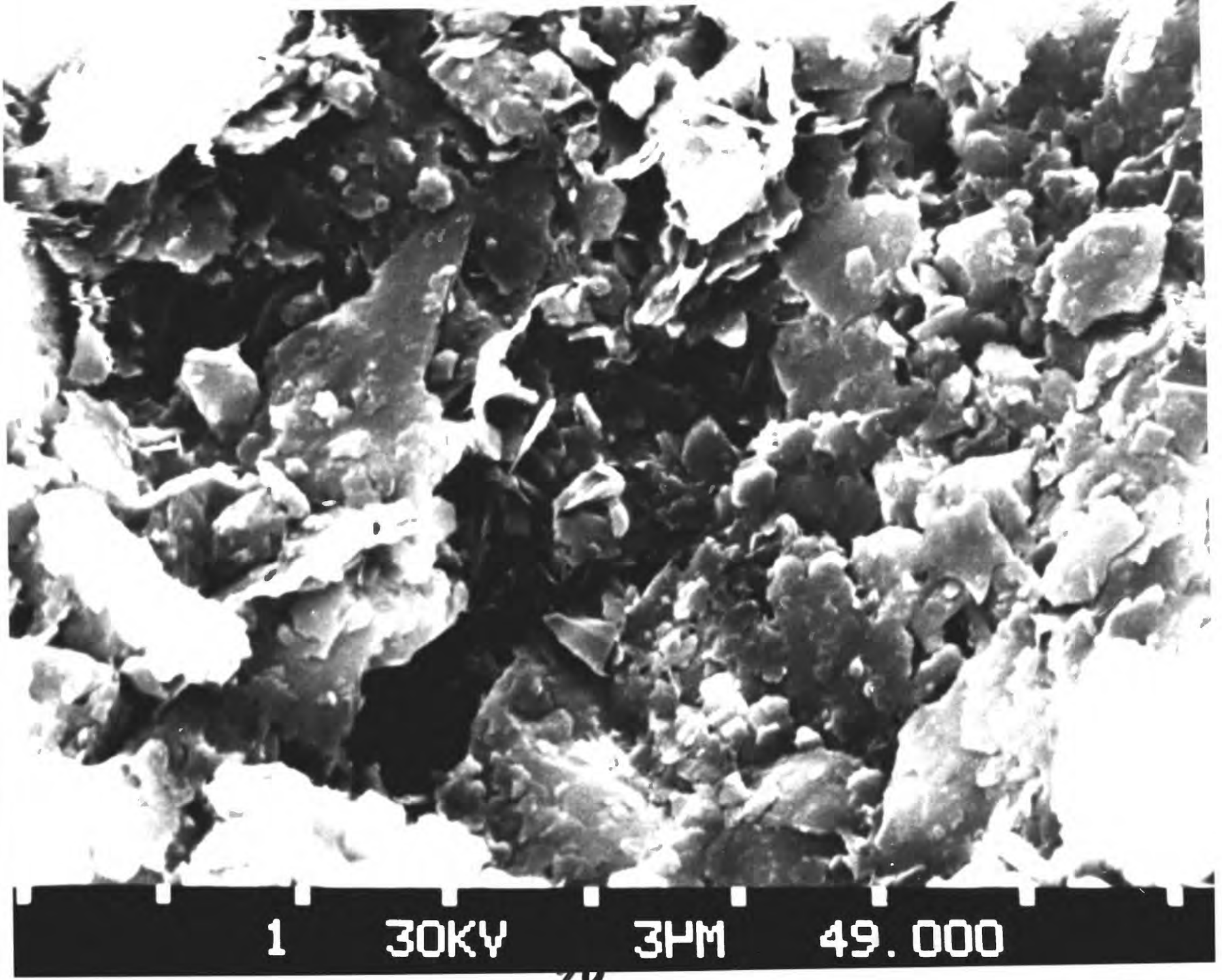
1 30KV 3MM 49.000

Figure 21. Facies F.III, normal to bedding planes, mag. = 5700X. Transassemblage void (tv) penetrating bedding oblique to plane of image.

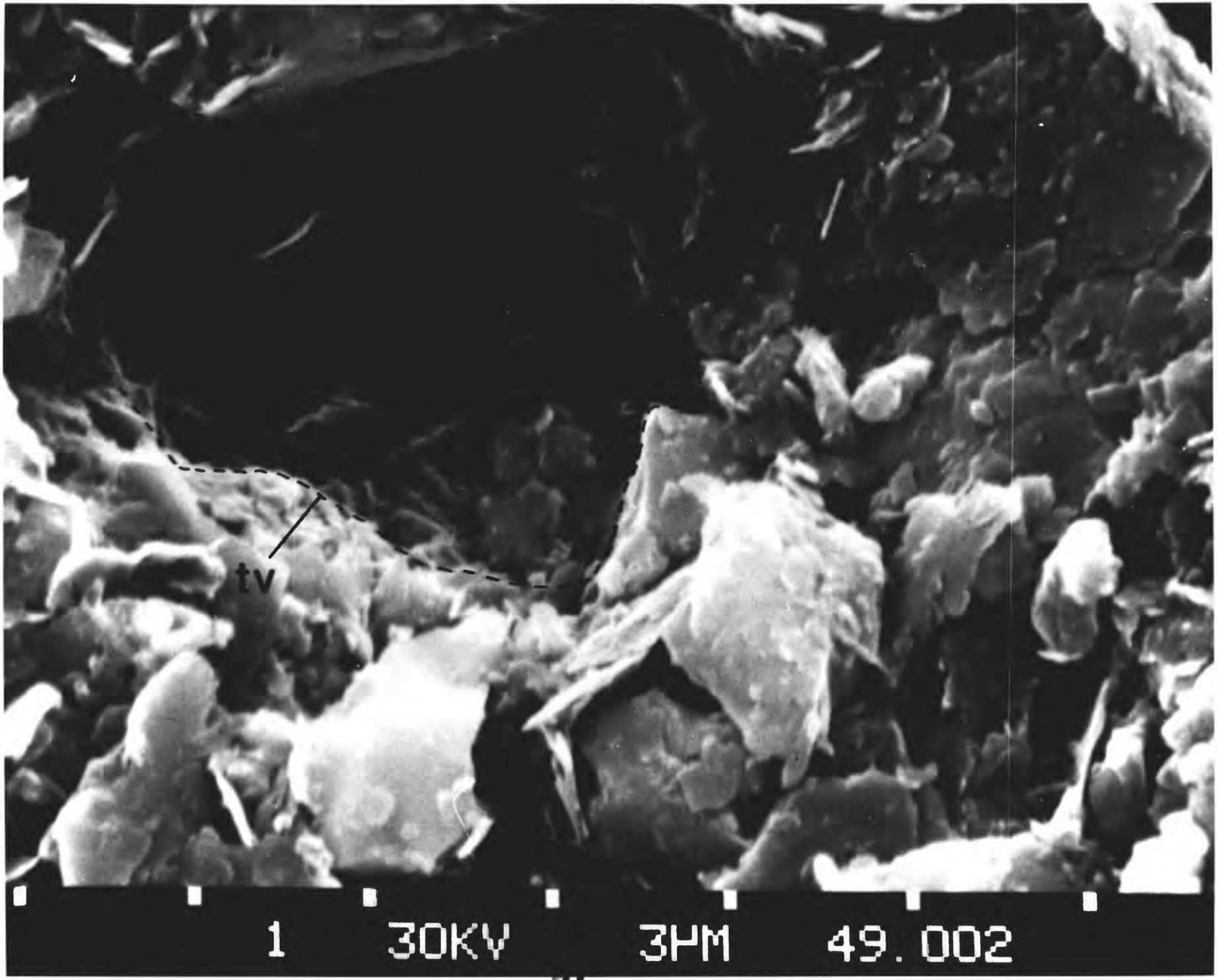
tv
1 30KV 3MM 49.002

Figure 22. Facies F.III, detail from figure 21, mag. = 15000X. Numerous clay grains normal to plane of image which contribute to metastable fabric.

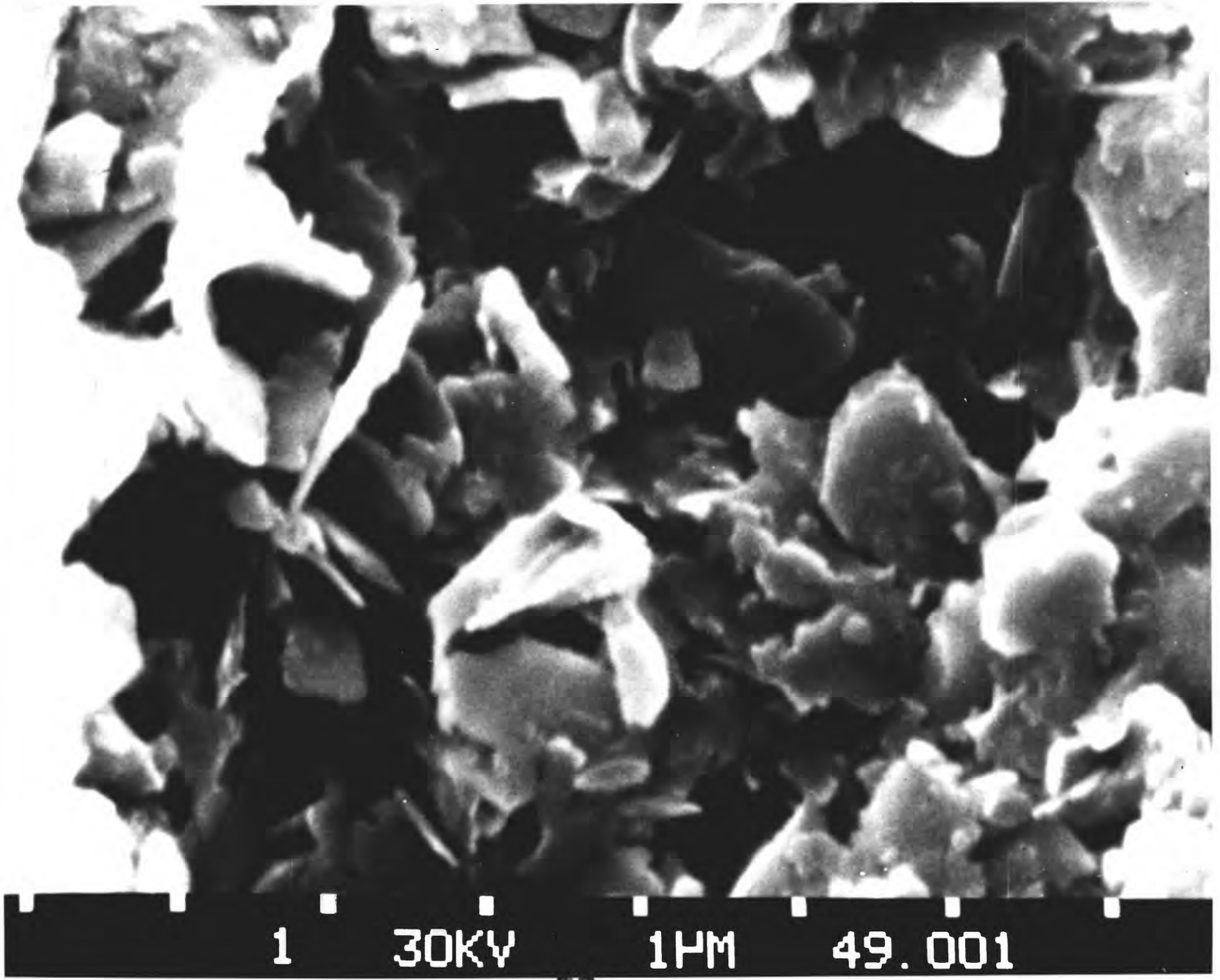
1 30KV 1PM 49.001

Figure 23. Facies F.III, parallel to bedding planes, mag. 2590X. General view showing silt grains (s) surrounded by open flocculated clay assemblages (of).

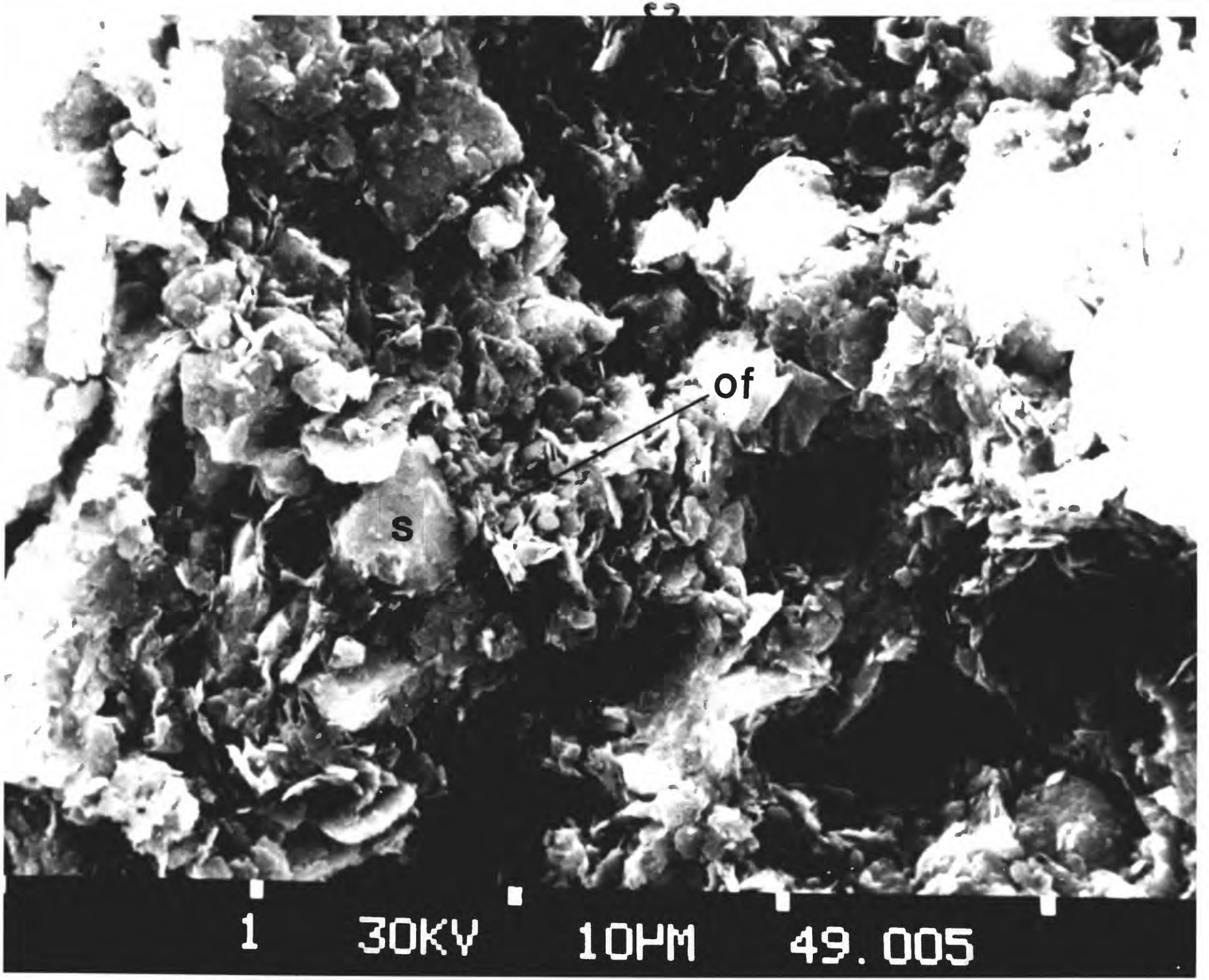
of
s
1 30KV 10UM 49.005

Figure 24. Facies F.III, parallel to bedding planes, mag. = 3200X. Honey-comb fabric (hc) well-developed with intervening areas comprised of flocculated aggregates (of) and random, rare silt grains (s).

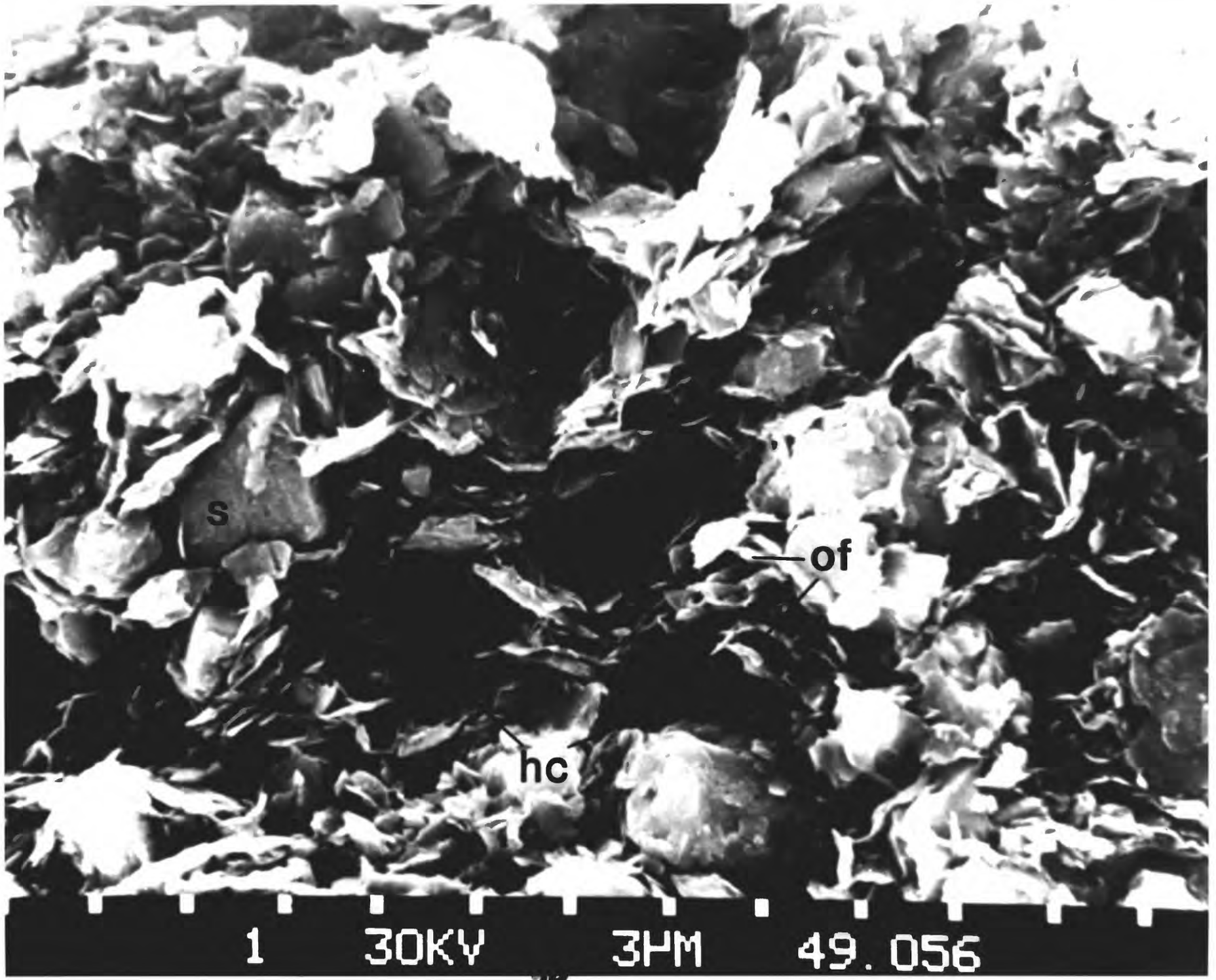
S
of
hc
1 30KV 3PM 49.056

Figure 25. Facies F.III, parallel to bedding planes, mag. = 4100X. Metastable fabric with incipient boxwork (bf). Note much of framework built from single clay grain-to-grain contacts.

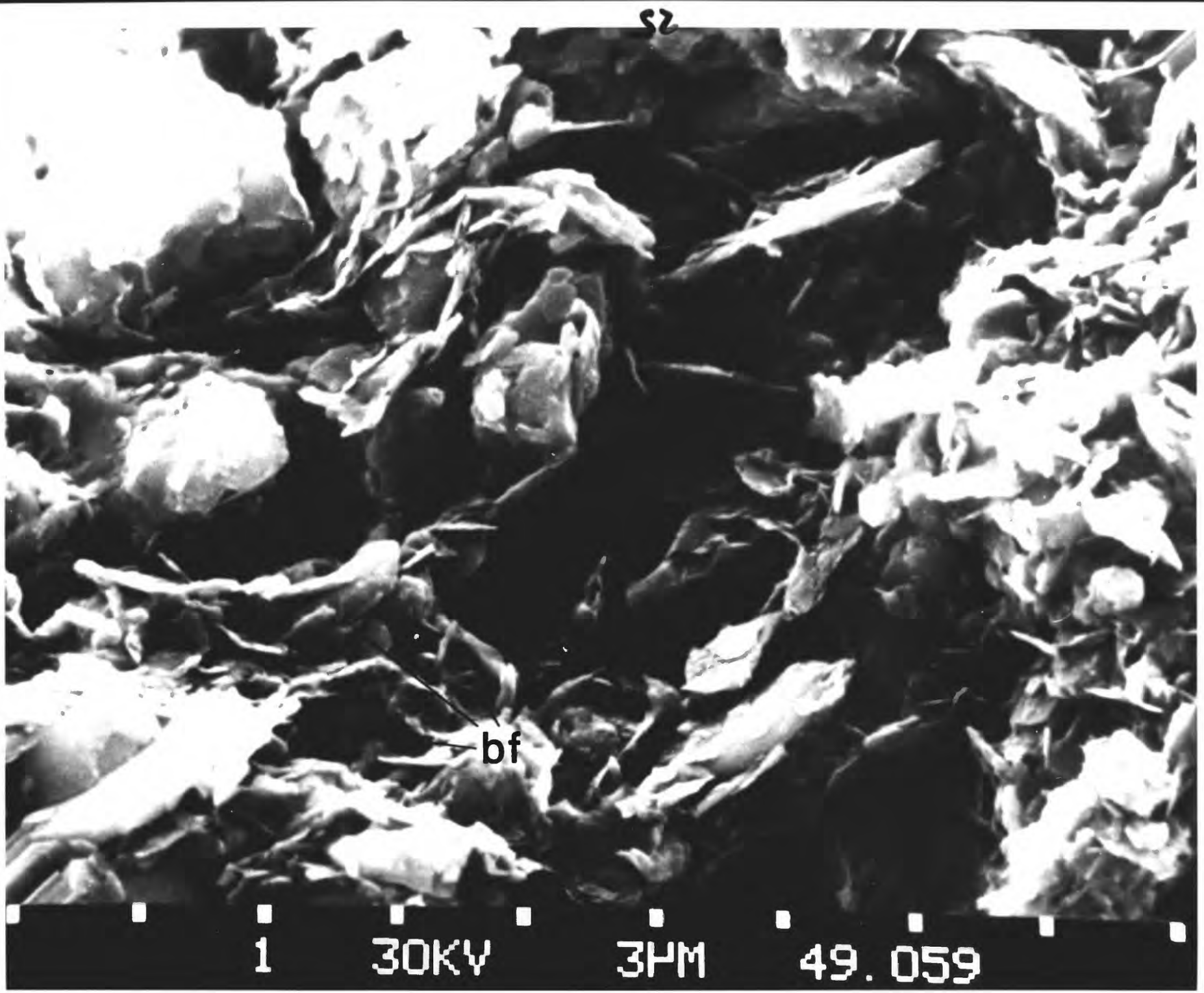
52
bf
1 30KV 3MM 49.059

Figure 26. Facies F.III, parallel to bedding planes, mag. = 4300X. Typical view of sensitive metastable fabric. Note dominance of clay. Bedding left to right, enhanced by collapsed zones (cz).

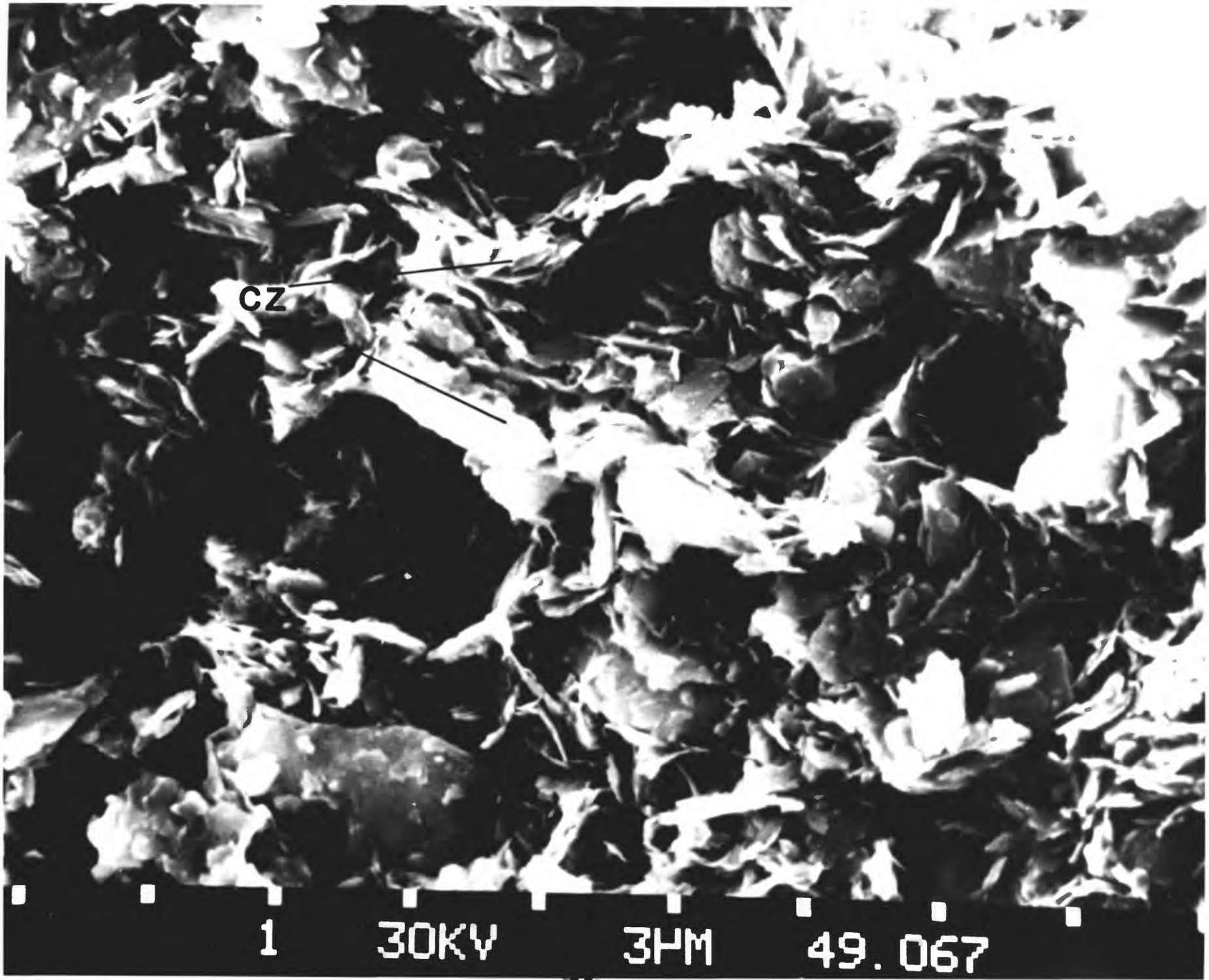
CZ
1 30KV 3MM 49.067

Figure 27. Facies F.III, parallel to bedding planes, mag. = 10,000X. High-magnification detail of figure 26. Bedding upper left to lower right. Note open fabric and attendant importance of normally-water-filled intra-assemblage voids (av) in conjunction with inter-assemblage voids (rv).

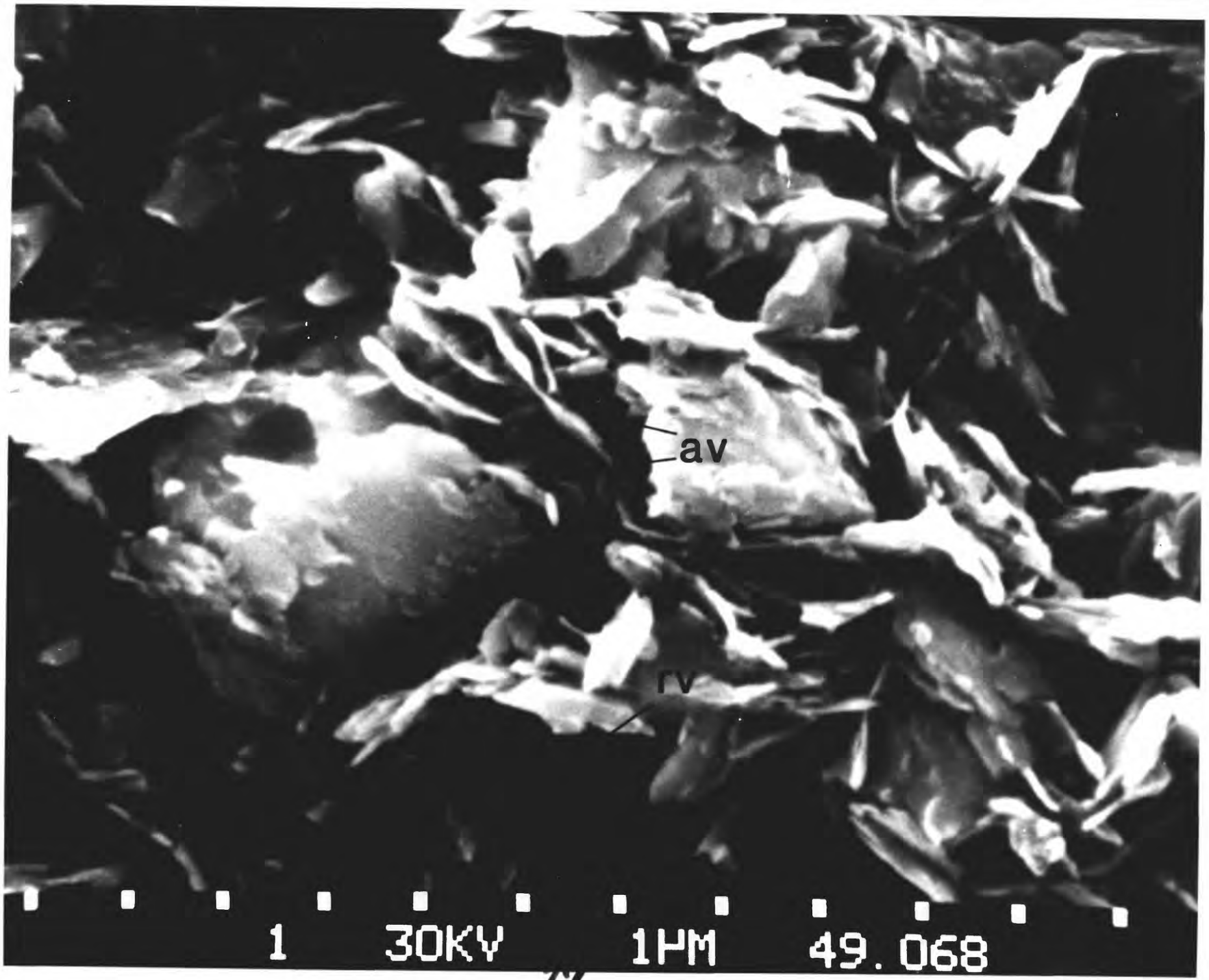
av
rv
1 30KV 1HM 49.068

Figure 28. Facies F.III, parallel to bedding planes, mag. = 5900X. Open box-work fabric (bf) with individual edge-to-edge (ee) and edge-to-face (ef) contacts between grains.

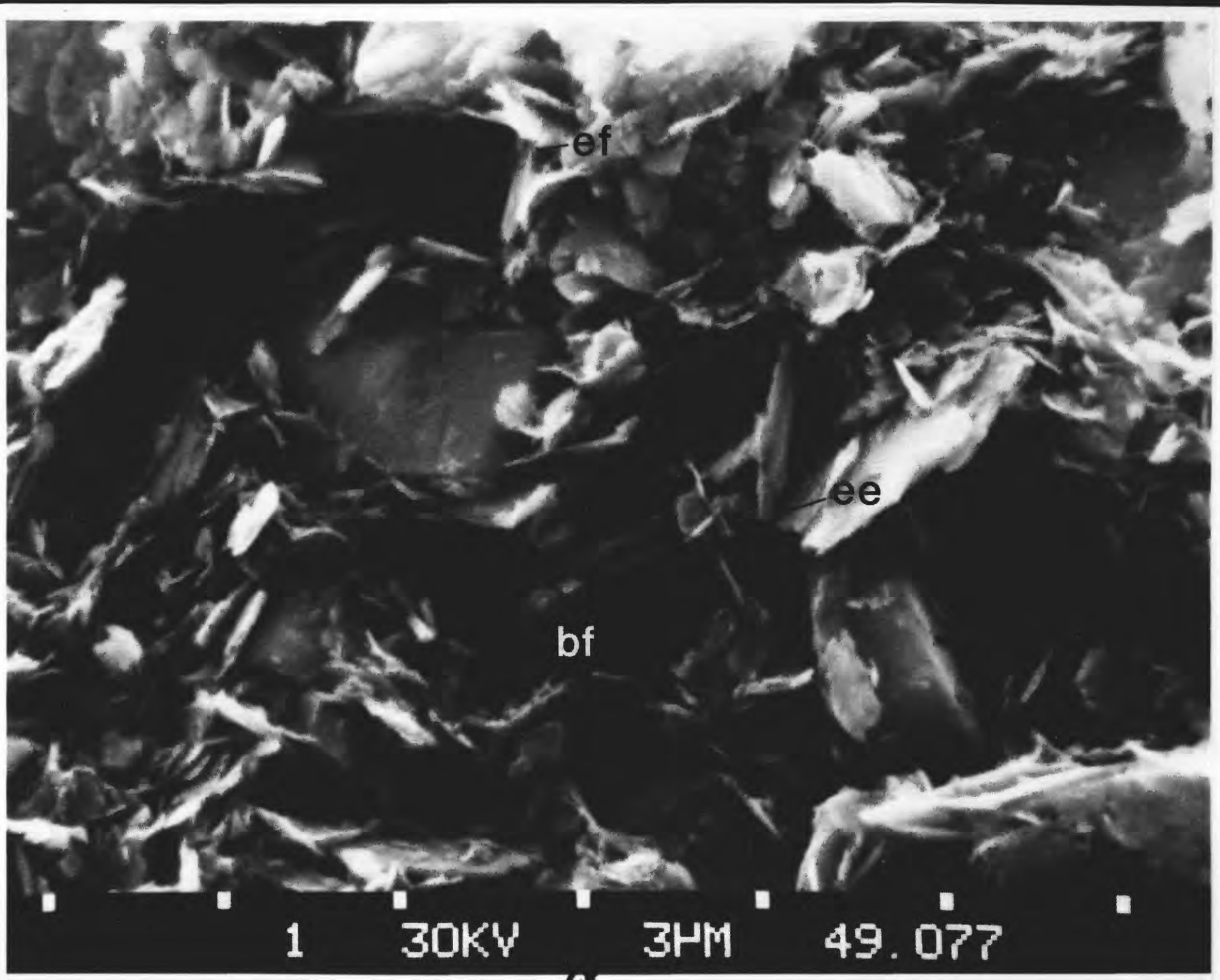
ef
ee
bf
1 30KV 3MM 49.077

Figure 29. Facies F.III, parallel to bedding planes, mag. = 10,000X. High sensitivity sample consisting of clay-coated silt grains (s) surrounded by flocculated clay fabric with edge-to-face (ef) and edge-to-edge (ee) contacts forming boxwork structure (bf).

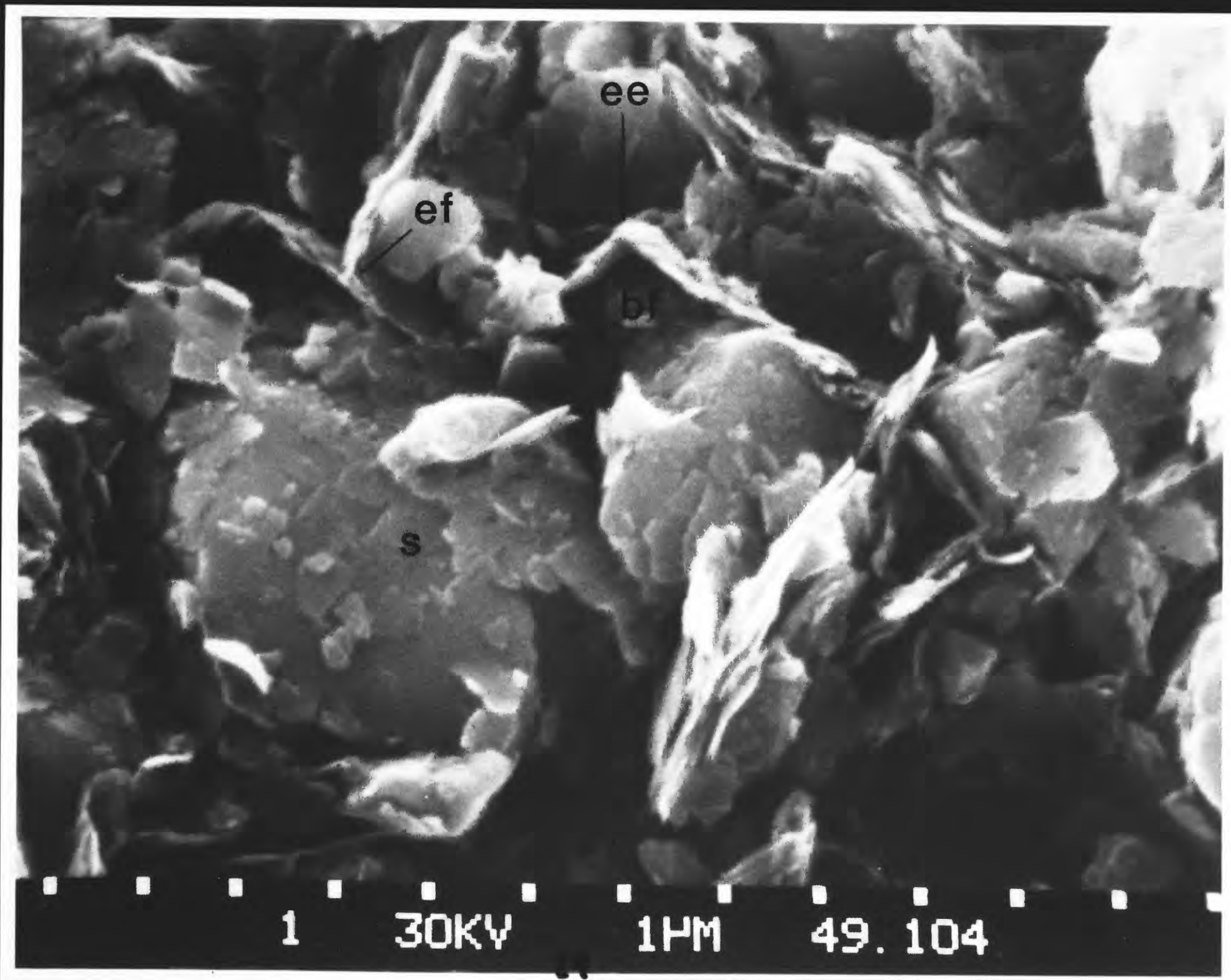
ee
ef
bl
s
1 30KV 1PM 49.104

Figure 30. Facies F.III, parallel to bedding planes, mag. 11,000X. Boxwork fabric (bf) consisting of edge-to-edge (ee) and edge-to-face (ef) contacts. Collapsed zone (cz) may represent shear plane.

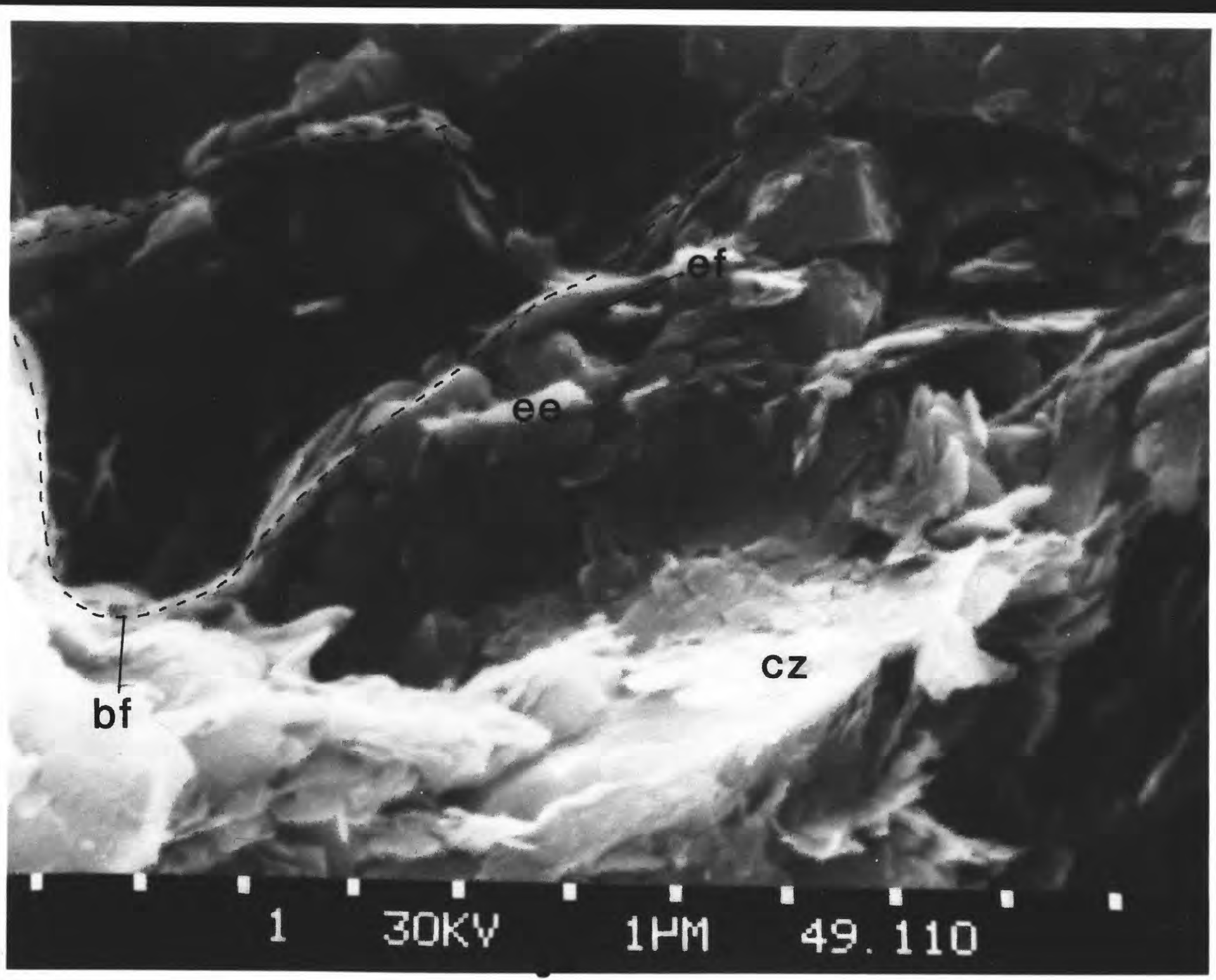
ef
ee
cz
bf
1 30KV 1PM 49.110

Figure 31. Facies F.III, parallel to bedding planes, mag. = 3500X. Bedding from upper right to lower left accentuated by dispersed fabric (df), separated by boxwork fabric (bf) and silt grains (s).

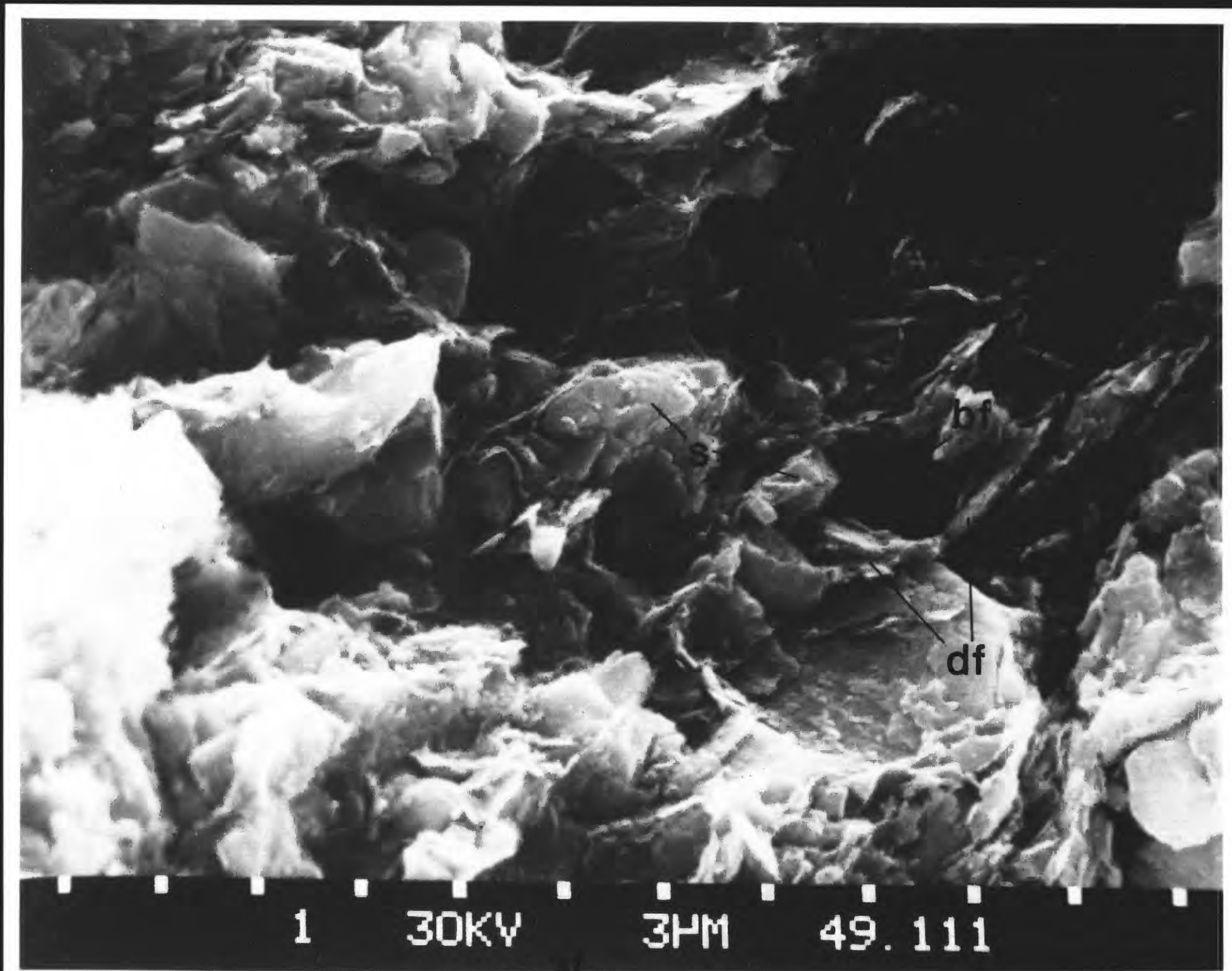
bf
s
df
1 30KV 3MM 49.111

Figure 32. Facies F.III, parallel to bedding planes, mag. = 20,000X. Close-up of high sensitivity sample fabric showing edge-to-face (ef)and edge-to-edge (ee) grain contacts.

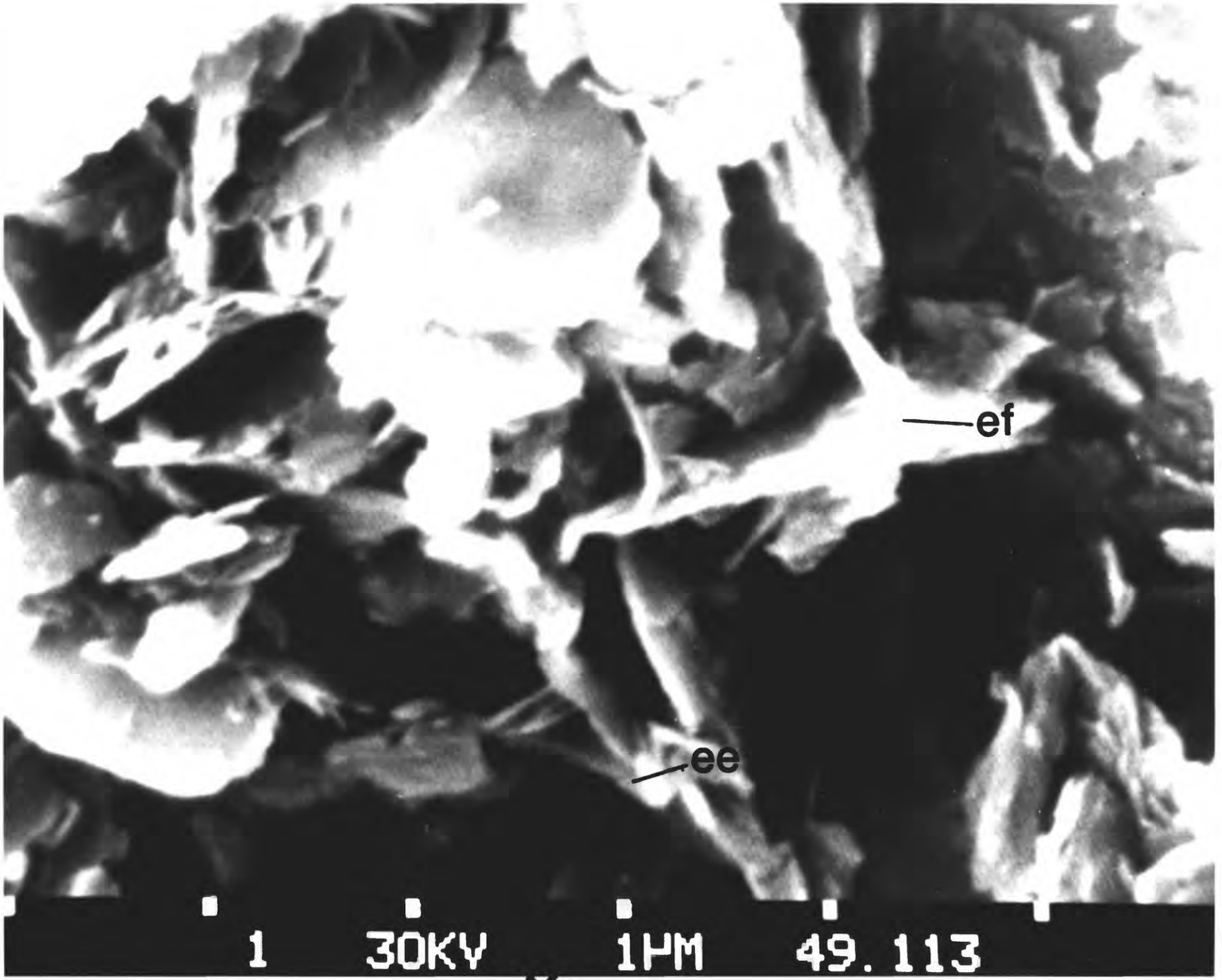
ef
ee
1 30KV 1MM 49.113

Figure 33. Facies F.III, parallel to bedding planes, mag. = 4300X. Bedding left to right. Fabric generally open and commonly boxwork (bf) of single platelet construction. Note collapsed zone (cz) trending diagonally. Silt is rare. See figure 34 for detail.

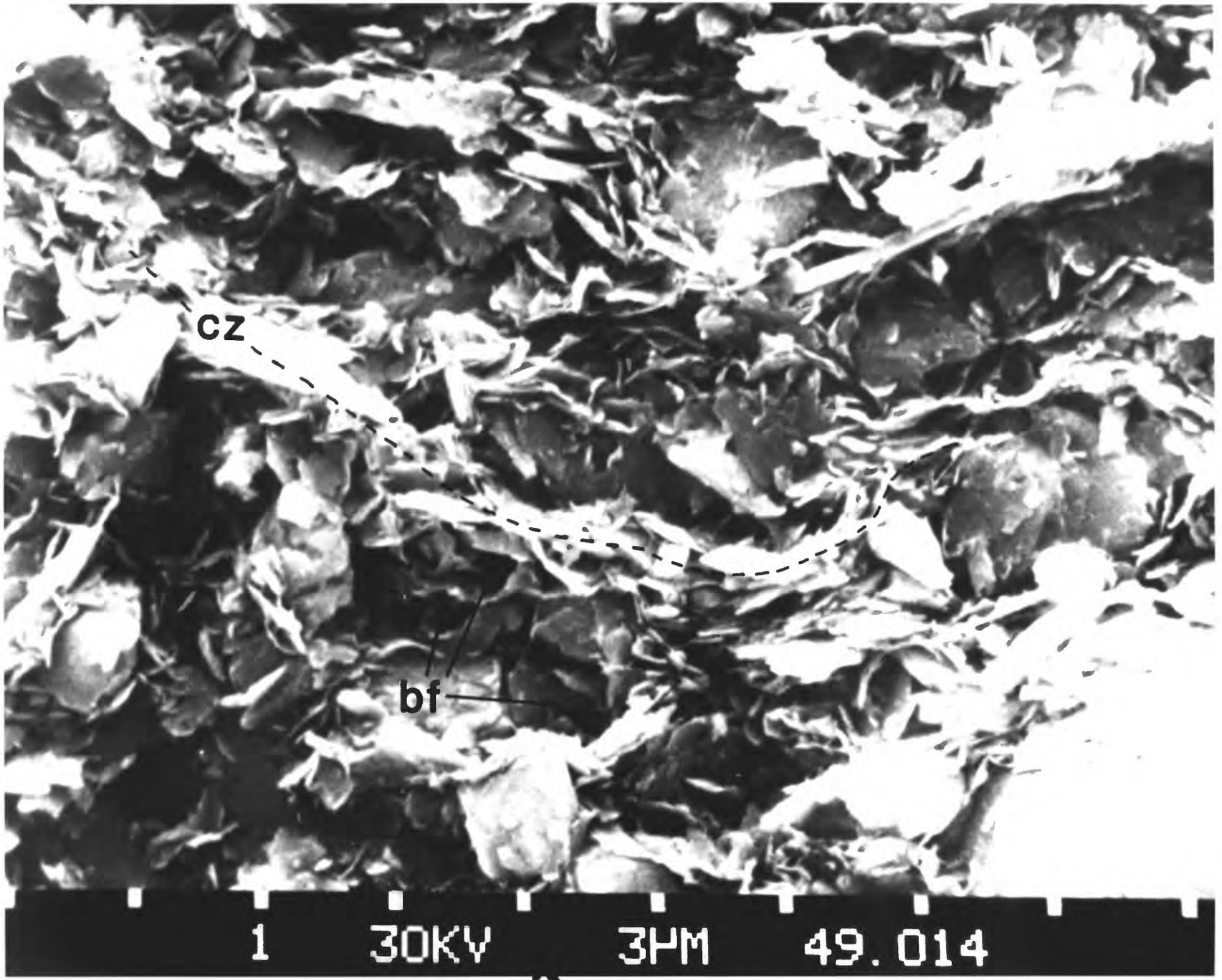
cz
bf
1 30KV 3MM 49.014

Figure 34. Facies F.III, detail of figure 33, mag. = 15000X. Collapsed zones (cz) surround small flocculated assemblage (of). Several examples of edge-to-face (ef) contacts.

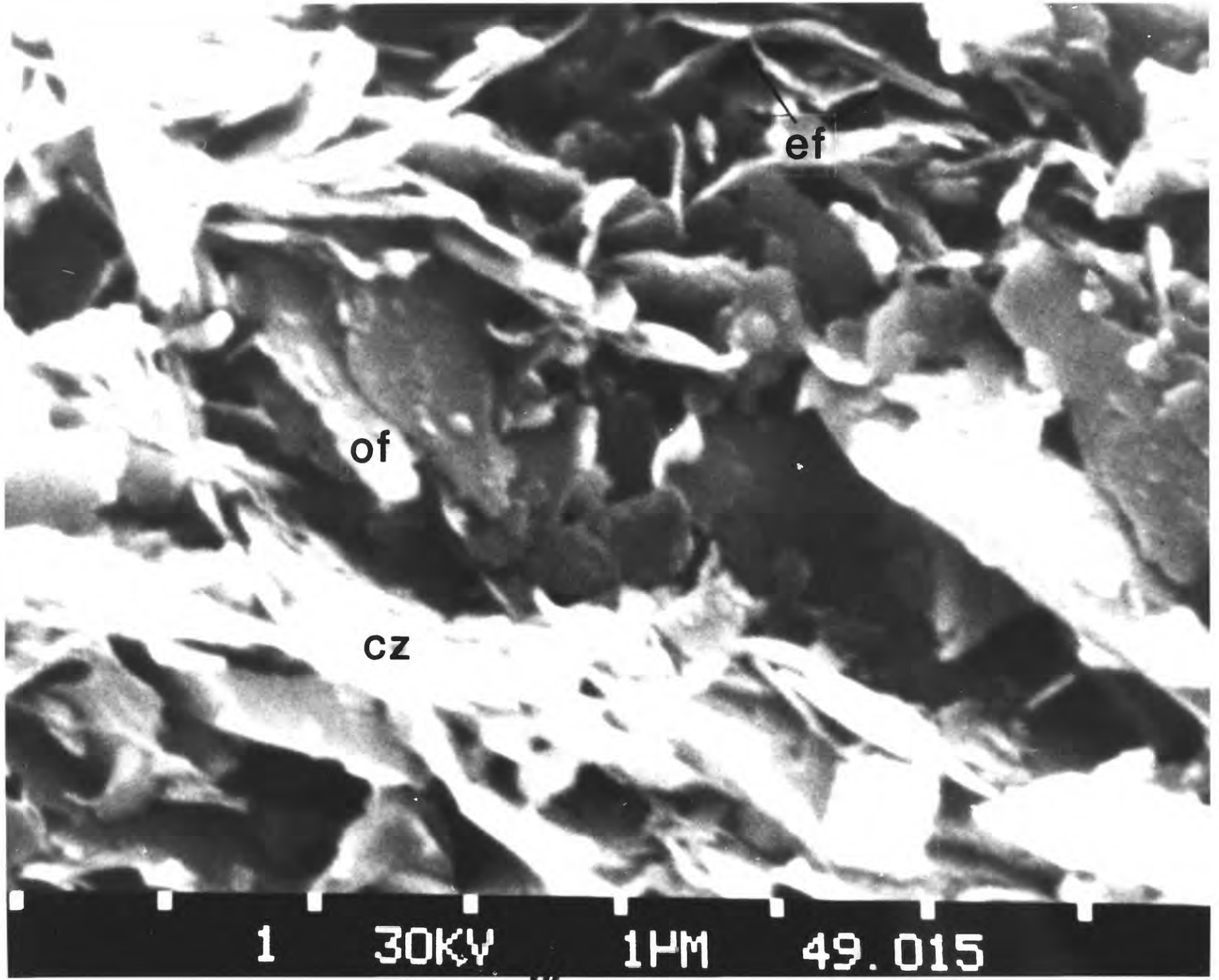
ef
of
cz
1 30KV 1HM 49.015

Figure 35. Facies F.III, parallel to bedding planes, mag. = 3200X. Bedding upper left to lower right. Clay honey-comb fabric (hc). Colloid floccules (cf) in bright areas. See figure 36 detail of blocked area.

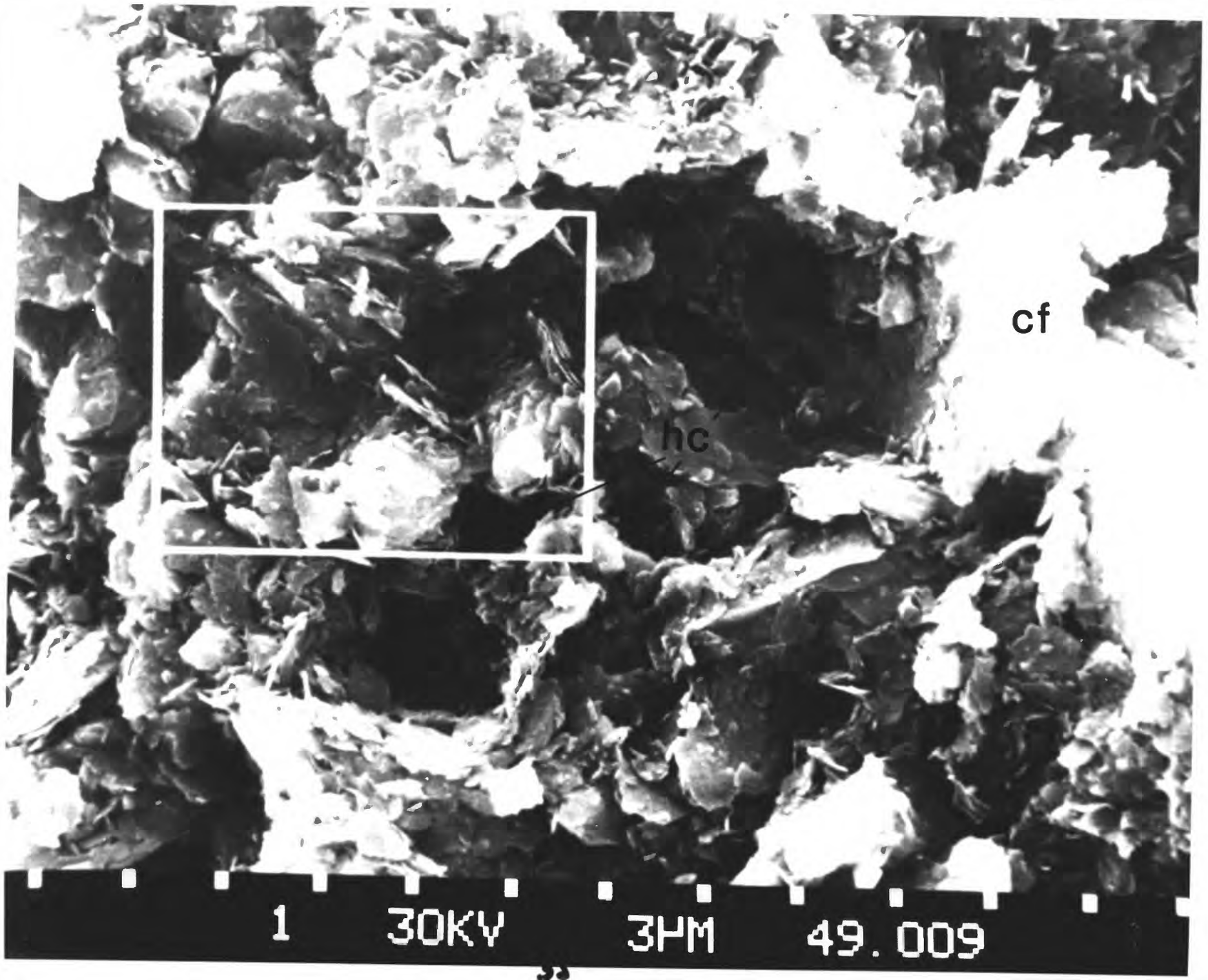
cf
hc
1 30KV 3MM 49.009

Figure 36. Facies F.III, detail from figure 35, mag. = 7800X. Collapsed and oriented clay grains indicate bedding attitude. Box-work fabric (bf) surrounds honey-comb void (hc).

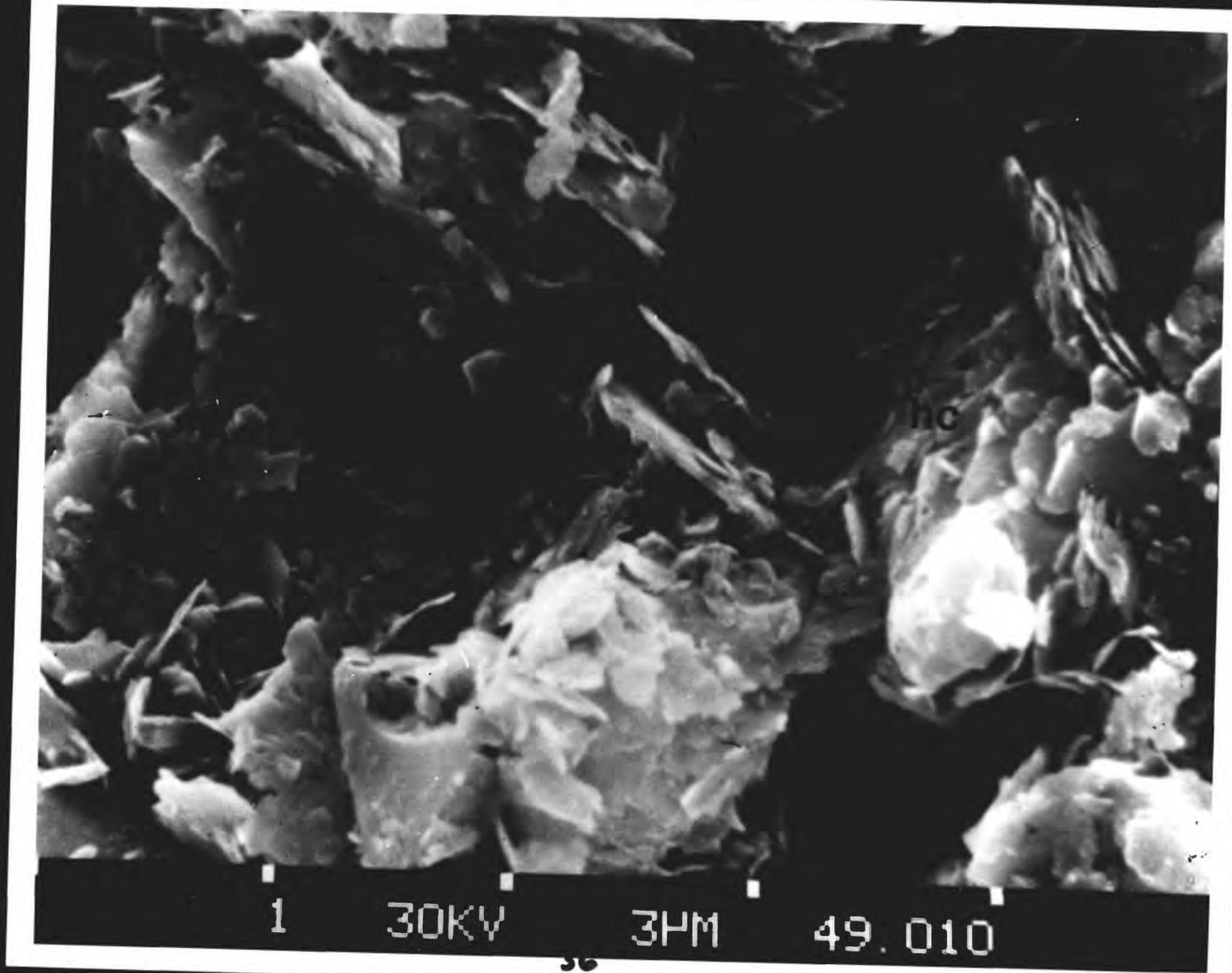
hc
1 30KV 3HM 49.010

Figure 37. Facies F.'III, parallel to bedding planes, mag. = 5000X. Stereoscopic view of high sensitive sample. Clay-coated silt grain at left, open flocculated fabric (of) at center.

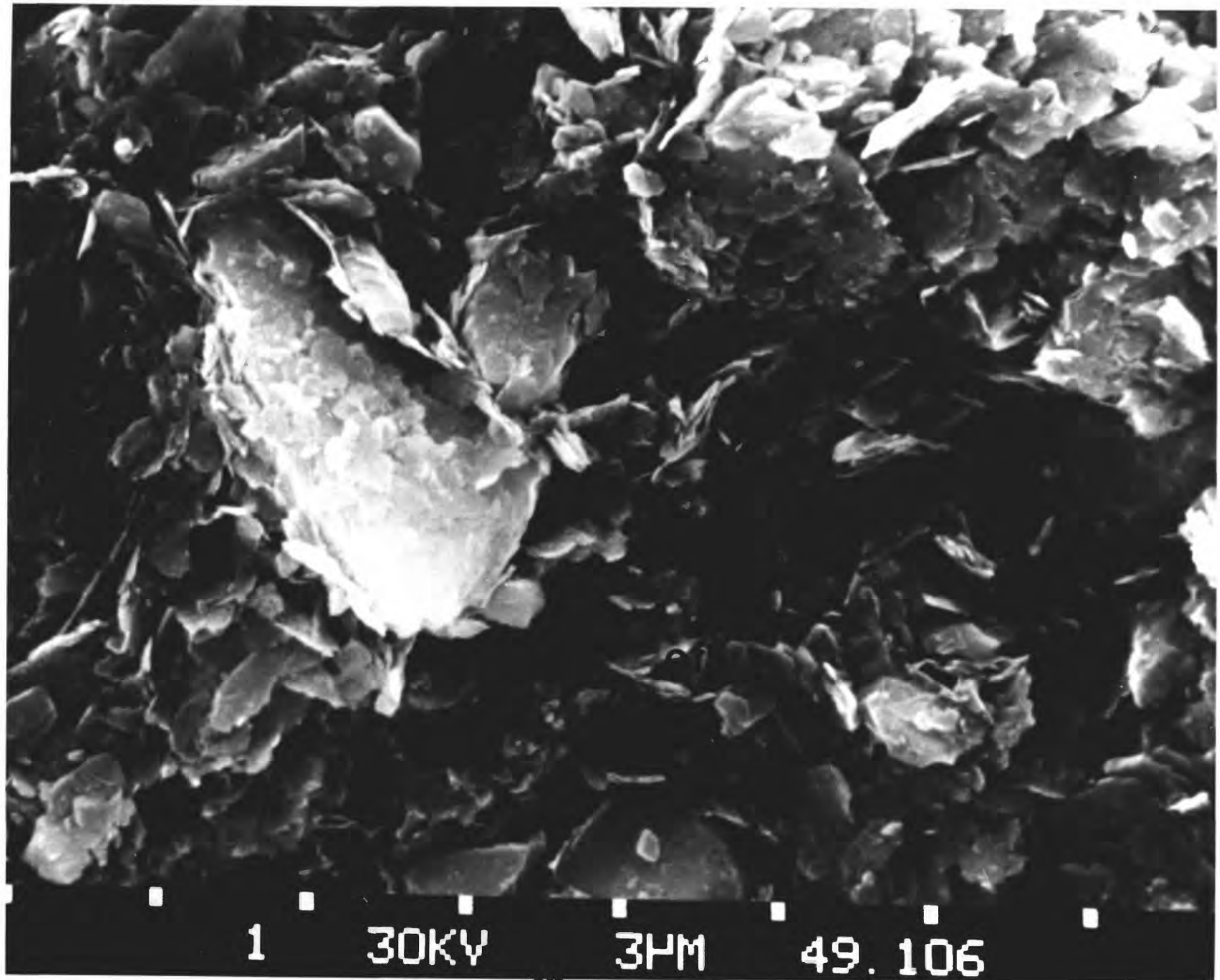
1 30KV 3PM 49.106

Figure 38. Facies F.IV, parallel to bedding planes, mag. = 3190X. Sample from a core which varied from low to moderate sensitivity. Bedding from upper left to lower right, with alternating silt and clay layers. Clay platelets vary from dispersed (df) to open flocculated (of) fabric in thin layers.

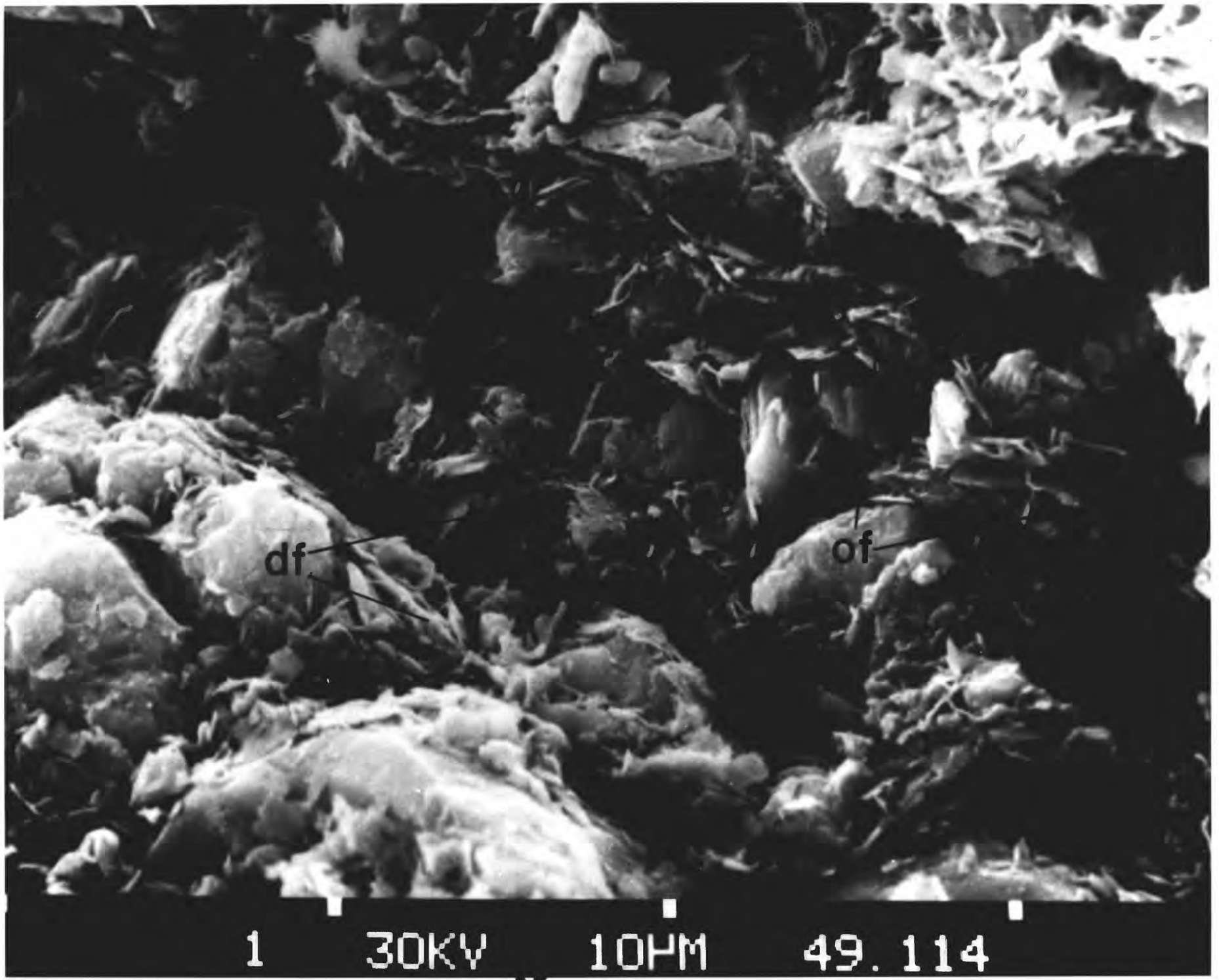
df
of
1 30KV 10UM 49.114

Figure 39. Facies F.IV, parallel to bedding plane, mag. = 3000X. Bedding from upper right to lower left. Alternating laminae of silt (s) and clay (c). Note clay fabric is collapsed.

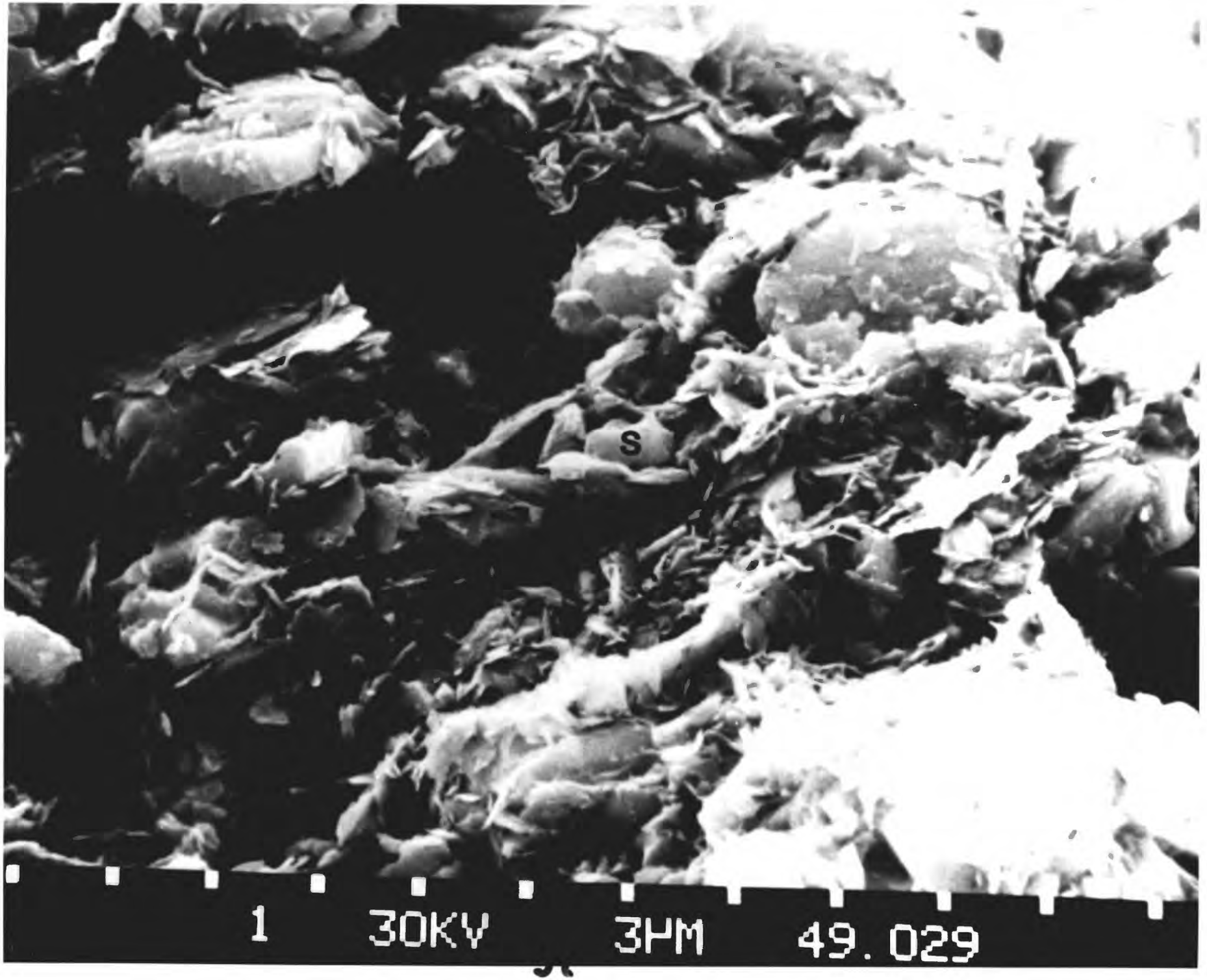
S
1 30KV 3PM 49.029

Figure 40. Facies F.IV, normal to bedding planes, mag. = 1010X. Connector assemblages (cc) contain fine silt in a compressed fabric. Large inter-assemblage voids (av).

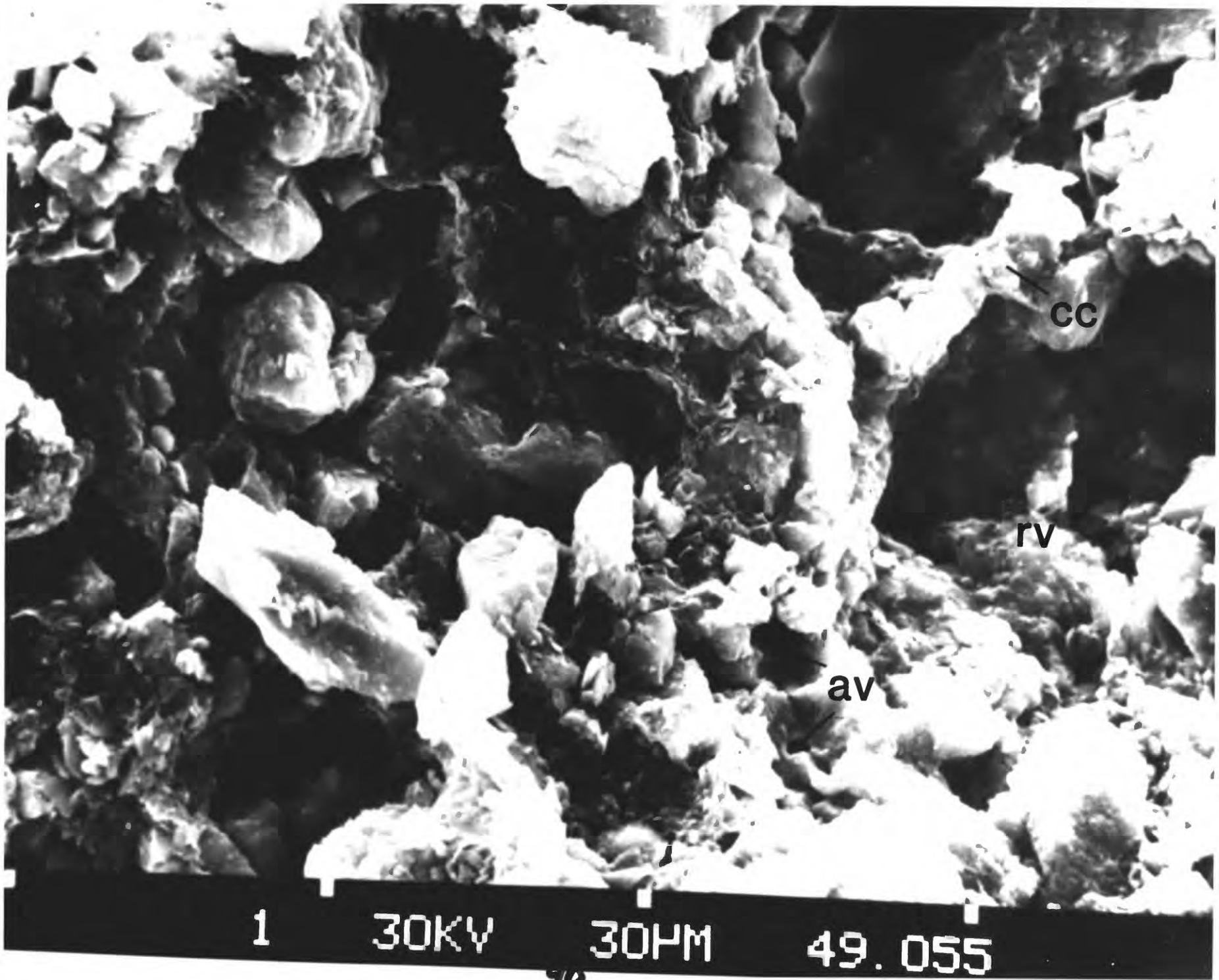
cc
rv
av
1 30KV 30HM 49.055

Figure 41. Facies F.IV, parallel to bedding plane, mag. = 5200X. Detail of sinuous clay connector assemblage between silt grains (s). Note intra-assemblage voids (av) and inter-assemblage voids (rv).

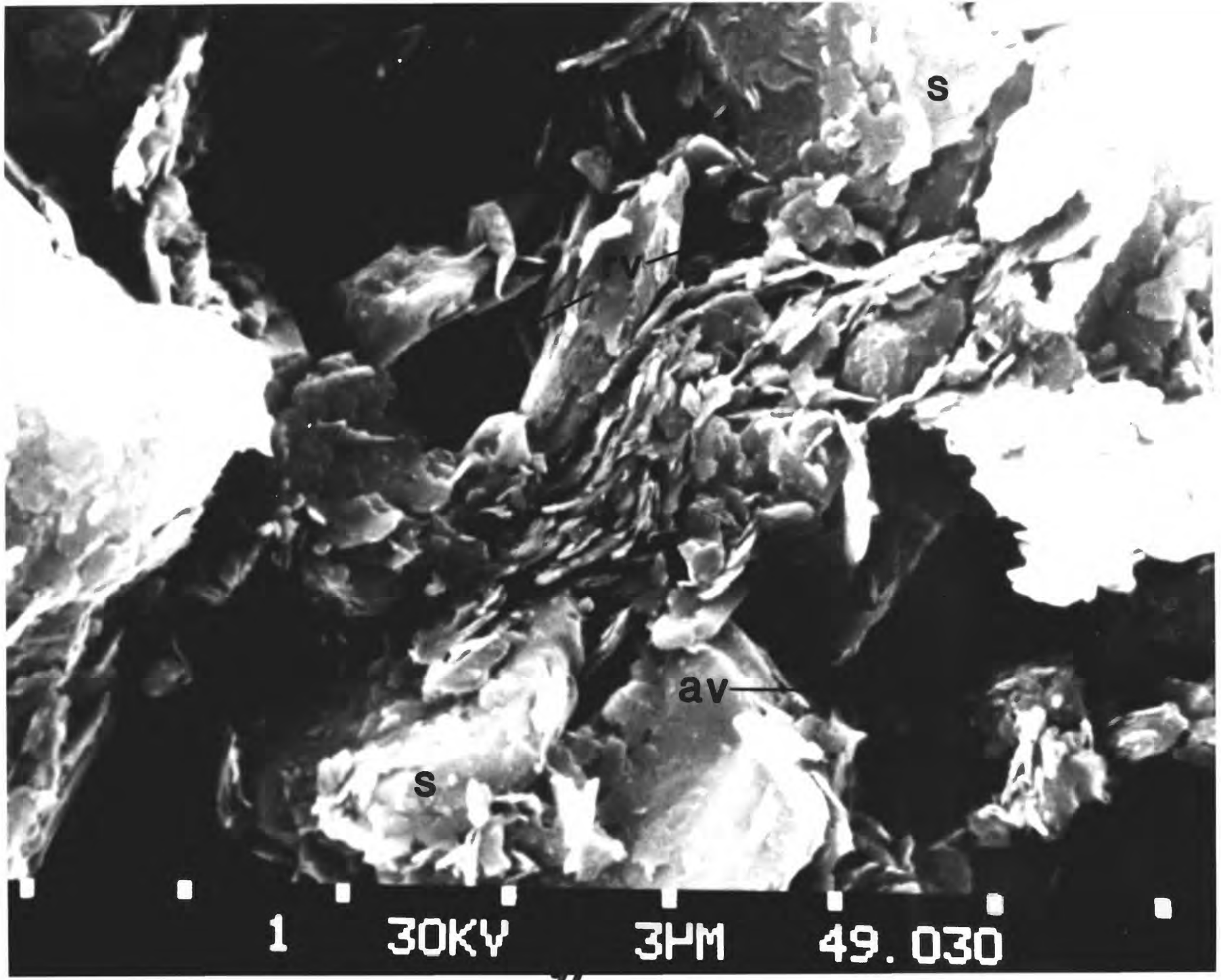
S
V
av
S
1 30KV 3MM 49.030

Figure 42. Facies F.IV, parallel to bedding planes, mag. = 5900X. Open-flocculated fabric in high sensitivity zone of a low sensitivity core (see fig. 38). Bedding from upper left to lower right. Note resultant high void ratio that results from boxwork fabric.

1 30KV 3MM 49 129

Figure 43. Facies F.V, normal to bedding plane, mag = 500X. Coarse silt and fine sand in compact silt and clay matrix. Note casts of removed clasts (k) and limited inter-assemblage voids (rv).

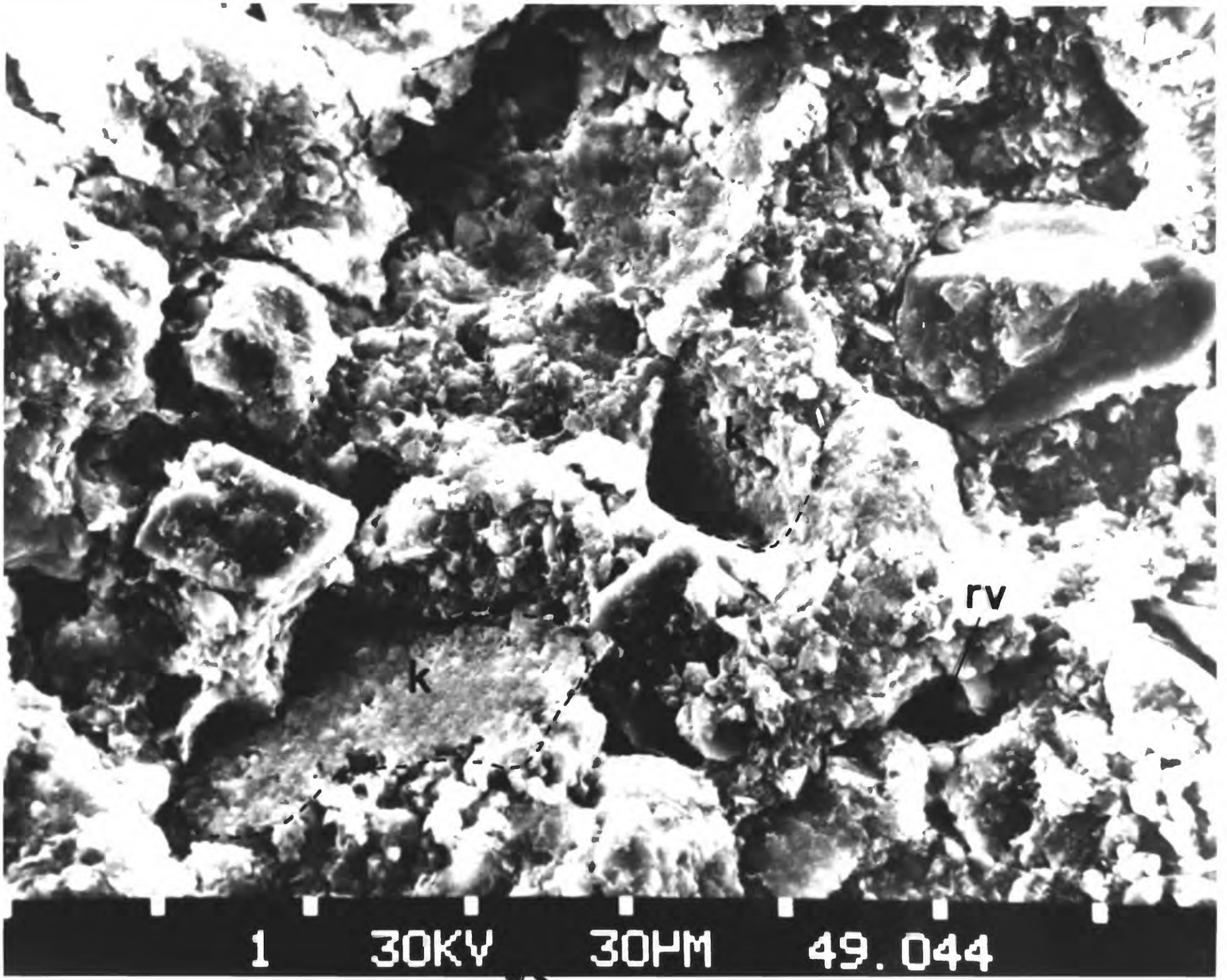
k
k
rv
1 30KV 30MM 49.044

Figure 44. Facies F.V, normal to bedding plane, mag. = 1360X. Higher magnification of compressed fine silt and clay fabric showing detail of casts from plucked coarser clasts (k).

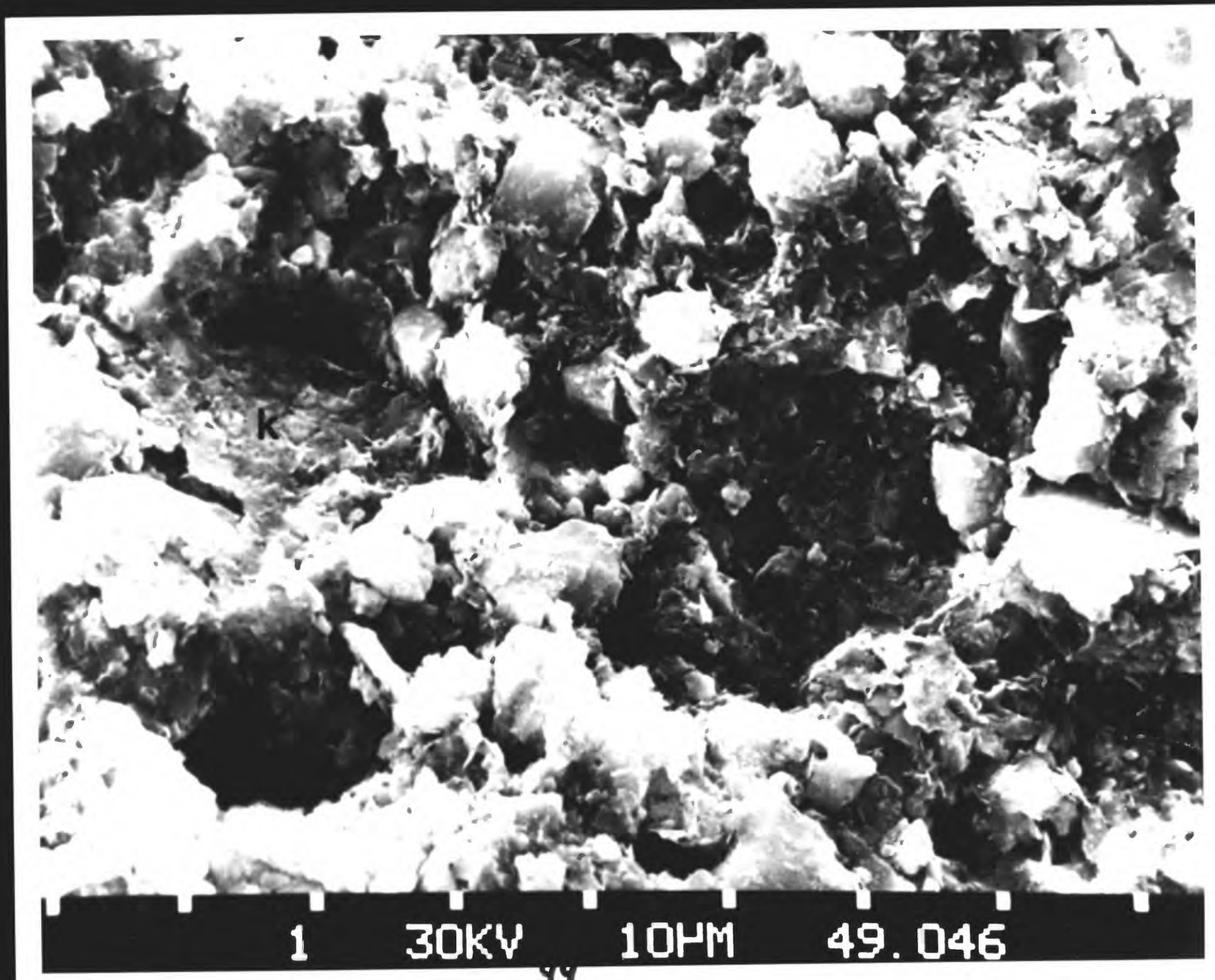
k
1 30KV 10UM 49.046

Figure 45. Facies F.VI within F.IV, normal to bedding plane, mag. = 320X. Medium to coarse silt, with fine sand. Note minor role of clay connector assemblages (cc), general angularity of grains, lack of cementation, and clean interparticle voids. Compare to figures 46, 47, and 48, at similar magnifications, which show clay connectors.

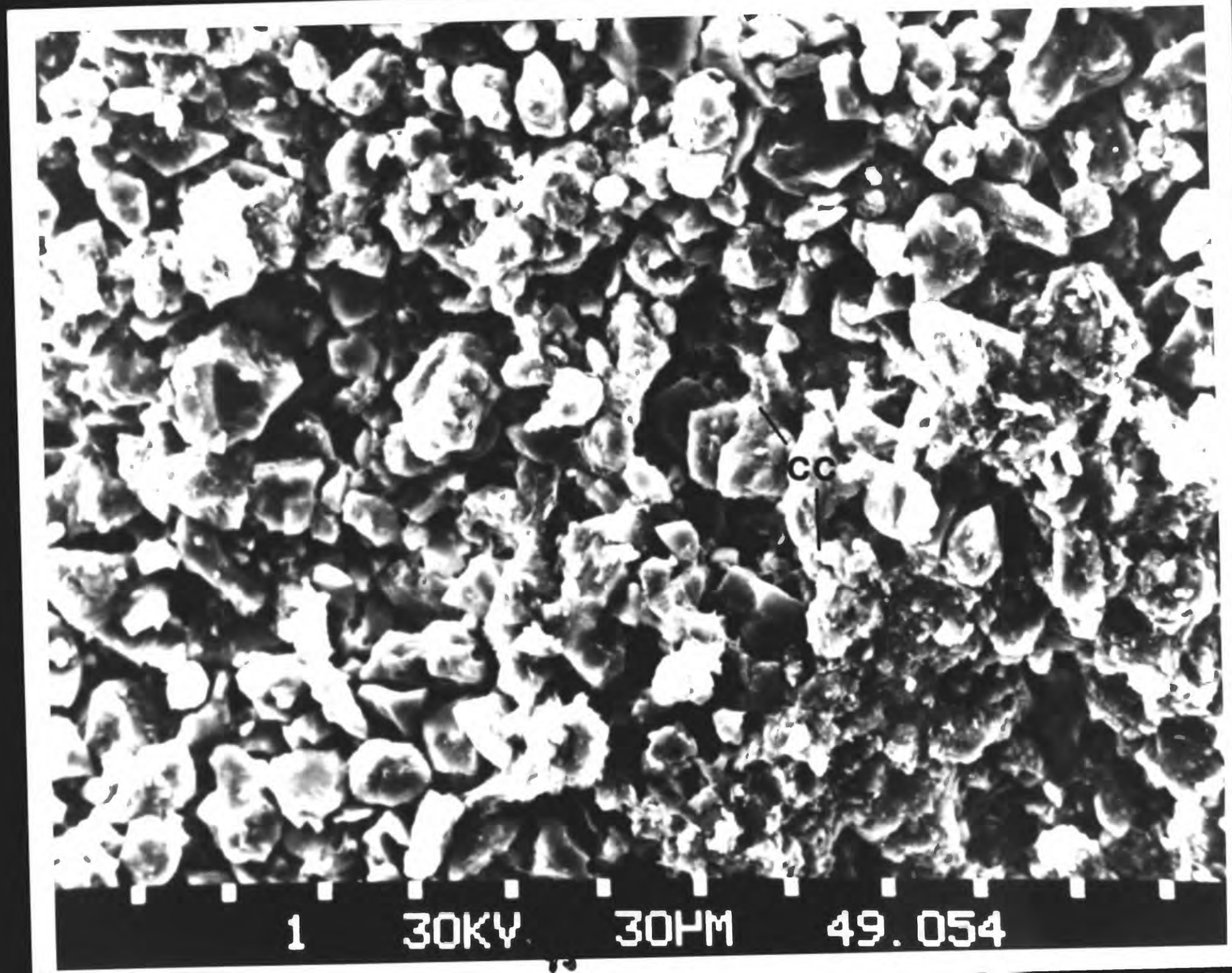
CC
1 30KV 30HM 49.054

Figure 46. Facies F.VI within F.IV, normal to bedding planes, mag. = 320X. Angular coarse silt to very fine sand in a compact fabric with grain-to-grain contacts and minor development of connectors (cc). Some chemical precipitates (cp) on grain surfaces. Compare to figures 45 and 47 at similar magnification.

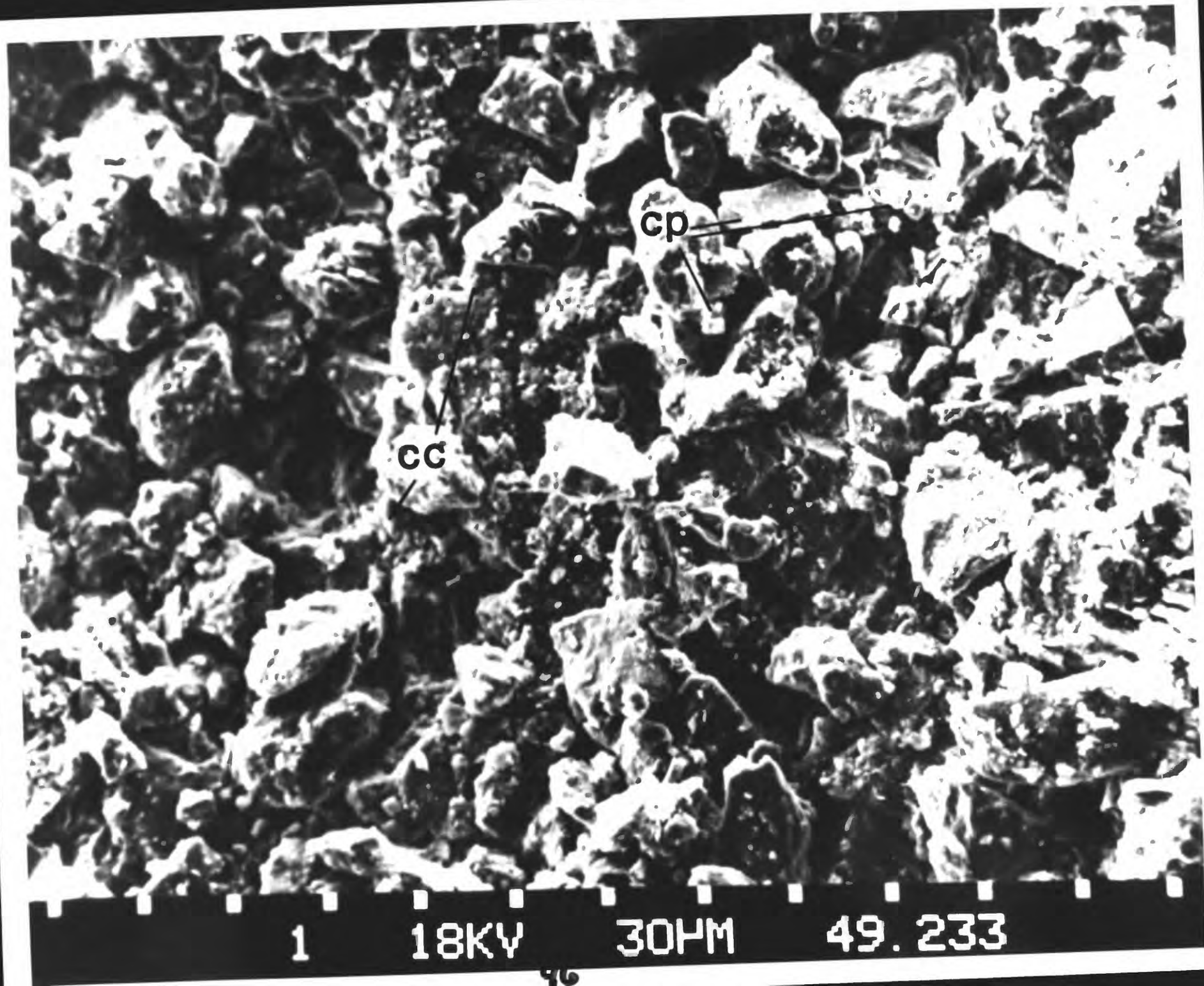
cp
cc
1 18KV 30HM 49.233

Figure 47. Facies F.VI within F.IV, parallel to bedding plane, mag. = 900X. Silt-dominant zone with chemical precipitate connectors. Bedding approximately left to right. See detail of boxed area in figure 48.

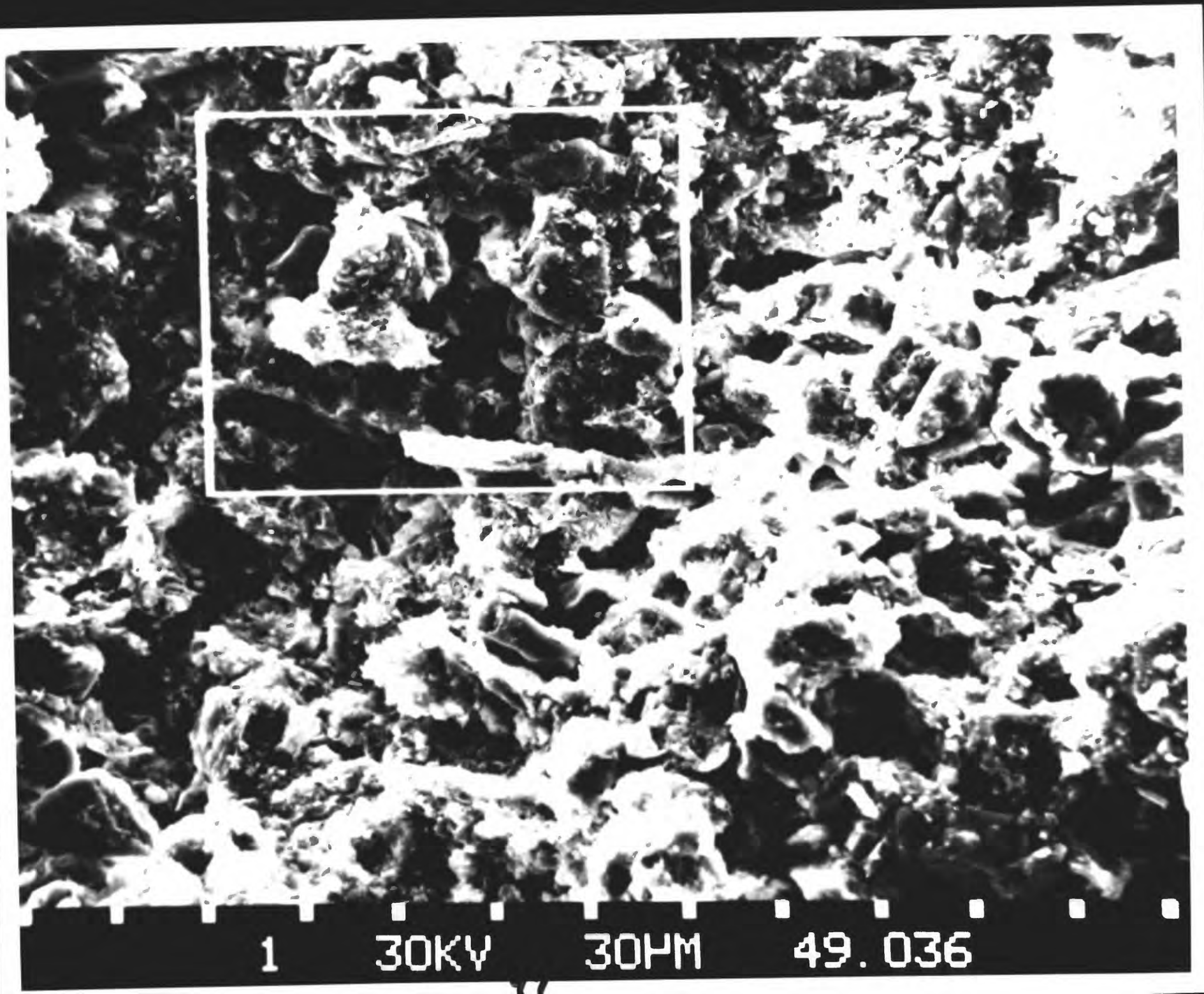
1 30KV 30UM 49.036

Figure 48. Facies F.VI within F.IV, detail of figure 47, mag. = 8400X. Coarse silt grains connected by clay-and-precipitate connector assemblage (cc). Clasts angular but commonly shrouded with fine silt and clay grains. Chemical precipitate composition is iron oxide based on EDAX determination.

30KV 30HM 49 028
1
CC